

1 **Characterizing tropospheric O<sub>3</sub> and CO around Frankfurt over**  
2 **the period 1994-2012 based on MOZAIC-IAGOS aircraft**  
3 **measurements**

4

5 **H. Petetin<sup>1</sup>, V. Thouret<sup>1</sup>, A. Fontaine<sup>1</sup>, B. Sauvage<sup>1</sup>, G. Athier<sup>1</sup>, R. Blot<sup>1</sup>, D.**  
6 **Boulanger<sup>1</sup>, J.-M. Cousin<sup>1</sup>, P. Nedelec<sup>1</sup>**

7 (1) {Laboratoire d'Aérodologie, Université de Toulouse, CNRS, UPS, France}

8 Correspondence to: H. Petetin (herve.petetin@aero.obs-mip.fr)

9 **Abstract**

10 In the framework of the MOZAIC-IAGOS program, vertical profiles of ozone (O<sub>3</sub>) and carbon  
11 monoxide (CO) are available since 1994 and 2002, respectively. This study investigates the  
12 variability and trends of both species in three tropospheric layers above the German airports  
13 Frankfurt and Munich. About 21,300 flights have been performed over the period 1994-2012, which  
14 represents the worldwide densest vertical in-situ dataset of O<sub>3</sub> and CO (with ~96 flights per month  
15 on average). The mean vertical profile of ozone shows a strong gradient in the first kilometre (due  
16 to dry deposition at ground and titration by NO) during the whole year and close to the tropopause  
17 (due to stratosphere-to-troposphere in-mixing) in spring and summer. The mean vertical profile of  
18 CO is characterized by high mixing ratios at ground, a strong decrease in the first kilometre, in  
19 particular in winter and autumn, and a moderate one in the free troposphere. O<sub>3</sub> minimizes in  
20 November-December and shows a broad spring/summer maximum in the lower and mid-  
21 troposphere and a sharp maximum in summer in the upper troposphere. The seasonal variation of  
22 CO shows a broad minimum in July-October close to the surface and in September-October higher  
23 in the troposphere, while the maximum occurs in February-April in the whole troposphere. Over the  
24 period 1994-2012, O<sub>3</sub> has changed insignificantly (at a 95% confidence level), except in winter  
25 where a slightly significant increase (from +0.83[+0.13;+1.67]% yr<sup>-1</sup> in the LT to  
26 +0.62[+0.02;+1.22]% yr<sup>-1</sup> in the UT, relatively to the reference year 2000) is found. The O<sub>3</sub> 5<sup>th</sup>  
27 percentile shows similar upward trends at the annual scale in all three tropospheric layers. All trends  
28 remain insignificant for the O<sub>3</sub> 95<sup>th</sup> percentile. In contrast, for CO the mean as well as its 5<sup>th</sup> and  
29 95<sup>th</sup> percentiles are decreasing both at the annual scale and at the seasonal scale in winter, spring  
30 and summer (although not always in all three tropospheric layers) with trends ranging between -  
31 1.22[-2.27;-0.47] and -2.63[-4.54;-1.42]% yr<sup>-1</sup>, relatively to the reference year 2004). However, all  
32 CO trends remain insignificant in autumn.

1 The phase of the seasonal variation of O<sub>3</sub> was found to change in the entire troposphere. The O<sub>3</sub>  
2 maxima moves forward in time with a rate of  $-17.8 \pm 6.0$  days decade<sup>-1</sup> in the lower troposphere, in  
3 general agreement with previous studies. Interestingly, this seasonal shift is shown to decrease with  
4 the altitude, with values of  $-7.8 \pm 2.5$  and  $-3.3 \pm 3.3$  days decade<sup>-1</sup> in the mid- and upper troposphere,  
5 respectively.

6

## 7 **1 Introduction**

8 As one of the major sources of hydroxyl radicals (OH) that directly control the atmospheric lifetime  
9 of a large number of compounds, ozone (O<sub>3</sub>) plays a unique role in the oxidative capacity of the  
10 atmosphere. In the troposphere, it acts as a powerful greenhouse gas with a positive radiative  
11 forcing (RF) of  $0.40 \pm 0.20$  W m<sup>-2</sup> that is not compensated by the RF of stratospheric ozone  
12 estimated at  $-0.05 \pm 0.10$  W m<sup>-2</sup> (IPCC, 2013). It also has well-known adverse impacts on human  
13 health (Jerrett et al., 2009), vegetation (Ashmore, 2005; Paoletti, 2006) and agricultural crop yields  
14 (Van Dingenen et al., 2009). In the troposphere, O<sub>3</sub> is formed by photochemical reactions implying  
15 various compounds including volatile organic compounds (VOC), carbon monoxide (CO) and  
16 nitrogen oxides (NO<sub>x</sub>). It can be removed by photolysis, dry deposition and uptake on aerosols  
17 (Moise and Rudich, 2000, 2002). Despite the considerable scientific achievements made during the  
18 last decades, the O<sub>3</sub> budget remains difficult to quantify precisely (Wu et al., 2007). Major  
19 uncertainties are related to lightning NO<sub>x</sub> production, isoprene biogenic emissions and degradation  
20 chemistry, biomass burning emissions, water vapour concentrations and stratosphere-troposphere  
21 exchange (STE) (Stevenson et al., 2006). This leads to a large heterogeneity of the O<sub>3</sub> abundance  
22 and variability in the troposphere, making it difficult to draw a simple and global picture of the O<sub>3</sub>  
23 present-day concentrations and trends.

24 During the last decades, O<sub>3</sub> trends in the free troposphere have been intensively investigated,  
25 notably based on long-term ozonesonde observations. Specifically in Europe where such  
26 measurements are available over a few decades at several sites (e.g., Hohenpeissenberg, Payerne,  
27 Uccle, De Bilt, Legionowo, Lindenberg), most results indicate an increase of ozone levels from the  
28 1960s until the mid-1980s (Logan et al., 1999; Oltmans et al., 1998; Tiao et al., 1986), the only site  
29 with no significant trend being Lindenberg, Germany, for the period 1975-1983 (Tiao et al., 1986).  
30 Such positive trends were found all along the year without any significant seasonal influence  
31 (Logan et al., 1999) and through the entire tropospheric column (Logan et al., 1999; Oltmans et al.,  
32 1998). By the mid-1980s until 2000s, most ozonesonde observations in Europe indicate a  
33 progressive levelling-off of ozone mixing ratios in the free troposphere (Logan et al., 1999; Oltmans  
34 et al., 1998, 2006; Gaudel et al., 2015). For instance, the significant positive trends obtained at  
35 Hohenpeissenberg in the entire tropospheric column for 1971-2010 vanish in most tropospheric

1 layers considering the period 1981-2010 (Oltmans et al., 2013). Ozone observations at Jungfraujoch,  
2 Switzerland (3850 m), an elevated alpine site supposed to be representative of the free troposphere,  
3 indeed reveal that mixing ratios have continued to increase in the 1990s, in particular during winter,  
4 the levelling-off occurring only in the 2000s (Cui et al., 2011). A similar evolution is reported by  
5 Cooper et al. (2014) at other mountain or remote sites in Europe, and by Logan et al. (2012) on the  
6 observations by the MOZAIC (Measurements of OZone and water vapour by Airbus In-service  
7 airCraft) aircraft above some European airports.

8 Observations at the coastal site Mace Head have shown an average annual increase of  $+0.25 \pm 0.09$   
9 ppb year<sup>-1</sup> of the baseline (i.e. originating from the Northern Hemispheric marine boundary layer)  
10 O<sub>3</sub> mixing ratios during the period 1988-2012 (Simmonds et al., 2004, Derwent et al., 2013). This  
11 increase has been the strongest in winter and spring and the lowest in summer, and has slowed  
12 down during the 2000s (Derwent et al., 2013). In contrast, the annual O<sub>3</sub> mixing ratios in European  
13 air masses have shown a much lower increase (Derwent et al., 2013), which suggests a possible  
14 compensation between a decrease of O<sub>3</sub> local formation in Europe and an increase of O<sub>3</sub> imports. At  
15 several remote or alpine sites in northern mid-latitudes, Parrish et al. (2013) recently highlighted a  
16 noticeable shift in the O<sub>3</sub> cycle at ground, the maximum daily O<sub>3</sub> occurring between 3 and 6 days  
17 earlier each decade since the 1970s. Such a shift may reflect some changes in the transport  
18 pathways, precursors emissions and photochemistry of O<sub>3</sub>, possibly due to climate change (Parrish  
19 et al., 2013).

20 The present study aims at characterizing the vertical distribution, the temporal variability, the  
21 seasonality and the trends of tropospheric O<sub>3</sub> in Central/Western Europe. Based on vertical profiles  
22 measured by commercial aircraft involved in the MOZAIC-IAGOS (In-service Aircraft for a Global  
23 Observing System) program, it will focus on the free and upper troposphere in order to go beyond  
24 the more limited representativeness in the boundary layer (BL) at the regional scale. However,  
25 results in the BL will be also presented to give a full picture of the troposphere. This study will also  
26 investigate the variability and trends of CO, one of the main O<sub>3</sub> precursors measured in the  
27 framework of the MOZAIC-IAGOS program. As a moderate lifetime (several weeks to several  
28 months) compound emitted by incomplete combustion processes, CO represents a powerful  
29 pollution tracer able to provide information on long-range transport at the hemispheric scale.  
30 Characterizing CO in troposphere may thus help investigating the variability and trends affecting O<sub>3</sub>.  
31 Section 2 presents the MOZAIC-IAGOS dataset and describes the treatment applied on vertical  
32 profile data. The vertical distribution, the seasonal variations, the trends of O<sub>3</sub> and CO and the  
33 changes affecting the O<sub>3</sub> seasonal cycle are analysed in Sect. 3. Main results and conclusions are  
34 summarized in Sect. 4.

## 1 **2 Data and methodology**

### 2 **2.1 MOZAIC-IAGOS dataset**

3 In the framework of the MOZAIC-IAGOS program ([www.iagos.org](http://www.iagos.org)), O<sub>3</sub> and CO measurements  
4 (among other parameters) are performed by commercial aircraft along various flight routes in the  
5 world (most of them from or to European airports) since 1994 (O<sub>3</sub>) and 2002 (CO), respectively  
6 (Marengo et al., 1998; Petzold et al., 2015). Until October 2014 (date of the last MOZAIC aircraft  
7 flight), both O<sub>3</sub> and CO have been measured using the same instruments in all aircraft, thus ensuring  
8 the dataset consistency during most of the period. Ozone measurements were performed using a  
9 dual-beam UV-absorption monitor (time resolution of 4 seconds) with an accuracy/precision  
10 estimated at about  $\pm 2$  ppbv /  $\pm 2\%$  (Thouret et al., 1998). Carbon monoxide was measured by an  
11 improved infrared filter correlation instrument (time resolution of 30 seconds) with an  
12 accuracy/precision estimated at  $\pm 5$  ppbv /  $\pm 5\%$  (Nédélec et al., 2003).

13 As MOZAIC aircraft have been retired from service, the European partners involved prepared since  
14 years the technical successor in the framework of the European Commission (EC) funded IAGOS  
15 program (Petzold et al., 2015). A new concept of aircraft system and instruments has been  
16 developed and installed on Airbus long-range aircraft (A340 or A330), starting from July 2011.  
17 Seven aircraft are actually in operation with IAGOS systems. The new IAGOS instrumentation for  
18 O<sub>3</sub> and CO is extensively described in Nédélec et al. (2015). The O<sub>3</sub> and CO measurements are  
19 based on the same technology used for MOZAIC, with the same estimated accuracy and the same  
20 data quality control. The nearly 4 years overlap of “historical” MOZAIC and “new” IAGOS  
21 instrumentation allowed to prove that the new IAGOS systems provide the same data quality  
22 (Nédélec et al., 2015), which is especially important for trends analysis.

23 Note also that several studies have investigated the consistency of the MOZAIC-IAGOS O<sub>3</sub> dataset  
24 with other types of in-situ data (e.g., surface stations, ozonesonde) (Logan et al., 2012; Staufer et al.,  
25 2013, 2014; Tanimoto et al., 2015; Zbinden et al., 2013). Focusing on O<sub>3</sub> changes in Europe, Logan  
26 et al. (2012) showed a reasonable agreement between aircraft and alpine sites but noticed the  
27 absence of O<sub>3</sub> increase in 1994-1998 in the sonde dataset (contrary to the two other types of data).  
28 Focusing on the pure tropospheric profiles, Zbinden et al. (2013) found a mean difference between  
29 MOZAIC-IAGOS and sondes of -2% in Germany, -8% in eastern United States and +1% over  
30 Japan. Tanimoto et al. (2015) obtained similar results, with differences between aircraft and sondes  
31 data around  $\pm 2\%$  throughout the whole troposphere in Belgium, Germany and Japan, and  $\pm 5\%$  at  
32 Hong Kong. The MOZAIC-IAGOS data at Munich were found to compare reasonably well with the  
33 surface observations at Hohenpeissenberg (slope of 0.97, correlation of 0.77).

34 The present study will focus on the airport Frankfurt where the longest (from 1994 to 2012) and  
35 densest (18,598 flights) record is available. In order to fill a large data gap in 2005, this dataset is

1 combined to the data from the airport Munich (2,734 flights, mostly between 2002 and 2005),  
2 approximately 300 km South-East from Frankfurt, as done in several previous studies (Logan et al.,  
3 2012; Zbinden et al., 2006, 2013). Note also that no measurements are available during a part of  
4 2010 due to instrumental problems. An illustration of the dataset density by month and year is  
5 shown in Fig. S1 and S2 in the Supplement.

## 6 **2.2 Tropopause altitude and tropospheric layers**

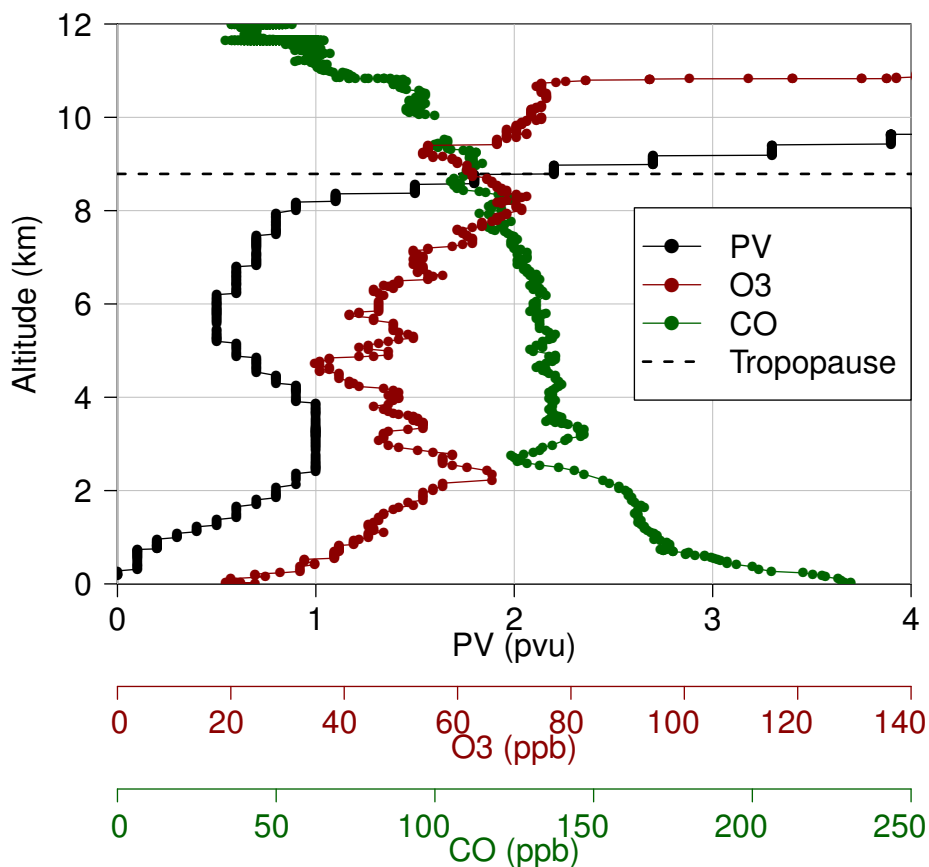
7 This paper focuses on the analysis of tropospheric vertical profiles obtained over Europe (Germany)  
8 during both ascent and descent. As tropospheric O<sub>3</sub> shows strongly varying sources, sinks and  
9 lifetimes with height, the troposphere is divided here in three layers: the lower troposphere (LT), the  
10 mid-troposphere (MT) and the upper troposphere (UT). As in Thouret et al. (2006), the UT is  
11 defined here as the layer having its top at the tropopause plus 15 hPa and spanning a pressure of 60  
12 hPa, that is a layer ~1.6 km thick and starting/ending ~2.1/~0.5 km below the tropopause. The MT  
13 is delimited by the UT lower boundary and an arbitrarily fixed altitude of 2 km. Data collected  
14 below are finally assigned to the LT, the first kilometre above surface being ignored to limit the  
15 representativeness degradation induced by emissions over the airport area (confirmed by large  
16 enhancements of CO mixing ratios near the ground in most vertical profiles). The influence of the  
17 local emissions on the observations in the LT will be briefly discussed in Sect. 3.2.2.

18 The tropopause altitude can be estimated by several approaches, e.g., thermal, dynamic, chemical  
19 criteria (Thouret et al., 2006) or a combination of them (Stohl et al., 2003b). In this paper, we  
20 consider the dynamical tropopause (DT), delimited by a potential vorticity (PV) of 2 pvu (1 pvu =  
21  $10^{-6} \text{ K m}^2 \text{ kg}^{-1} \text{ s}^{-1}$ ) (see the tropopause height over the period 1994-2012 in Fig. S3 in the  
22 Supplement). Two parameters, the PV and the pressure at which PV reaches 2 pvu (so-called  $p_{\text{PV}=2}$ ),  
23 are derived along all MOZAIC flight routes based on the European Centre for Medium-Range  
24 Weather Forecasts (ECMWF) operational analysis (00:00, 06:00, 12:00, 18:00 UTC) and forecasts  
25 (03:00, 09:00, 15:00, 21:00 UTC). The pressure at the DT ( $p_{\text{PV}=2}$ ) plus 15 hPa defined the top of the  
26 UT applied here.

27 Tropospheric vertical profiles are selected according to several criteria:

- 28 (i) Distance from the airport: Take-offs and landings do not exactly correspond to vertical  
29 profiles as aircraft travel some distance before reaching their cruise altitude. In order to  
30 limit the uncertainties induced by a potential horizontal heterogeneity, a maximum distance  
31 of 400 km from the airport is fixed for the vertical profile data selection. In practice, such a  
32 distance is sufficient for sampling the entire vertical profile in most flights, and remains  
33 reasonable considering the fact that the O<sub>3</sub> vertical variability is expected to be higher than  
34 the horizontal one. A sensitivity test with a distance threshold of 800 km leads to  
35 differences of mean O<sub>3</sub> mixing ratio in the UT below 3% at the seasonal and annual scale.

1 (ii) Potential vorticity: Based on PV vertical profiles, the 2 pvu value is used to locate the top of  
 2 the tropospheric vertical profiles. This is illustrated in Fig. 1 with the flight from Frankfurt  
 3 to Boston on the 19 March 2002 during which the DT altitude is estimated at 8.8 km. If the  
 4 distance criterion is fulfilled before reaching DT, the  $p_{PV=2}$  parameter is used to estimate the  
 5 DT pressure (and thus to determine to which tropospheric layer points belong). However,  
 6 PV values above 2 pvu may sometimes be encountered in the lower troposphere — due to  
 7 recent deep stratospheric intrusions or convective processes — before decreasing again  
 8 below the 2 pvu threshold until the tropopause. To avoid a misevaluation of the DT  
 9 altitudes in such cases, PV values are not considered point by point but over a window of  
 10 several points — in our case, 60 points, which approximately corresponds to 1800 m on the  
 11 vertical — and the tropopause is considered to be reached only when the minimum PV over  
 12 that window exceeds 2 pvu (this value of 60 being empirically chosen to handle most of  
 13 these situations) (or when the previous criteria is fulfilled) and is set to the bottom of that  
 14 window. In this study, we are thus considering the real and not purely tropospheric layer,  
 15 i.e., recent stratospheric intrusions are not filtered in our methodology.



16  
 17 Figure 1: Vertical profile of the potential vorticity (PV), O<sub>3</sub> and CO mixing ratios during the flight  
 18 from Frankfurt to Boston on the 19 March 2002 (take-off). The tropopause altitude (dotted black  
 19 line) is estimated based on PV (see text for the methodology).

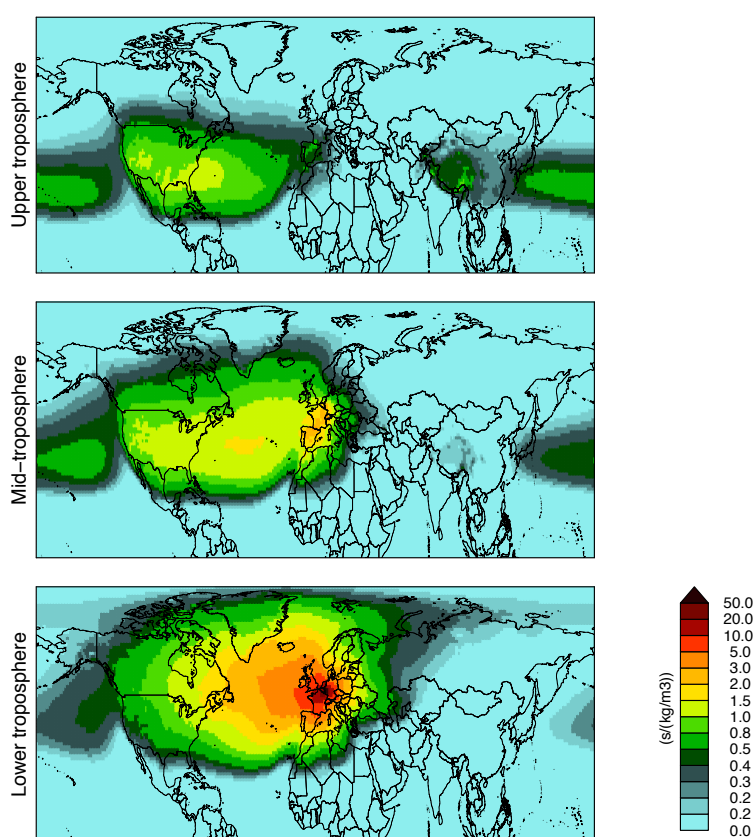
1 It is worth noting that the determination of the tropopause altitude is associated to several  
2 uncertainties. Some uncertainties arise from the choice of the method used to locate the tropopause.  
3 For instance, the chemical tropopause (defined in terms of both O<sub>3</sub> mixing ratio and vertical  
4 gradient of O<sub>3</sub> mixing ratio, also referred as the ozone tropopause) is on average below the thermal  
5 tropopause (Bethan et al., 1996). In the determination of the DT altitude, other uncertainties can  
6 arise from the choice of a constant PV to locate the DT. Indeed, Kunz et al. (2011) showed that the  
7 PV values at the DT can vary between 1.5 and 5, with higher PV values in summer than in winter.  
8 In our case, there are also uncertainties related to the fact that the PV is here a modelled variable. In  
9 addition, it is linearly interpolated between PV fields 6-hours apart, which does not allow to entirely  
10 catch the variability of the DT. A good example is given in Fig. 1 where the abrupt O<sub>3</sub> increase  
11 (corresponding to the tropopause) occurs 2 km above the DT derived from PV values. However, our  
12 approach allows to assess in which layer (MT or UT) observations belong even when the  
13 tropopause is not reached (within the 400 km around the airport). In order to assess the uncertainties  
14 introduced by an erroneous DT pressure, we compared it with the pressure at which the O<sub>3</sub> mixing  
15 ratio reaches 150 ppb (taken here a simplified estimate of the chemical tropopause) and remains  
16 above at higher altitude (in order to avoid stratospheric intrusions in the troposphere). This was  
17 done on all vertical profiles where it was possible, which represents 46% of the dataset. On average  
18 over the period 1994-2012, the mean bias of the DT pressure compared to the 150 ppb O<sub>3</sub>-isopleth  
19 is +21 hPa, while the 5<sup>th</sup>, 10<sup>th</sup>, 90<sup>th</sup> and 95<sup>th</sup> percentiles of this bias are -72, -32, +78 and +99 hPa,  
20 respectively. Therefore, the DT derived from PV values tends to be located below the 150 ppb O<sub>3</sub>-  
21 isopleth, which may bias low the O<sub>3</sub> mixing ratios in the UT. However, the discrepancy remains  
22 moderate on most profiles. It is beyond the scope of this study to investigate in more details the  
23 influence of the method used to locate the tropopause. Above the airport Frankfurt, a majority of  
24 vertical profiles (63%) reach the tropopause while most of the remaining profiles (36%) are selected  
25 according to the distance criteria. A similar proportion is found at Munich (63 and 35%,  
26 respectively).

27

### 28 **2.3 FLEXPART simulations**

29 The FLEXPART Lagrangian particle dispersion model (Stohl et al., 2005) is used to investigate the  
30 origin of air masses sampled by the aircraft in the different tropospheric layers above  
31 Frankfurt/Munich. Input meteorological data are taken from the ECMWF operational analysis  
32 (00:00, 06:00, 12:00, 18:00 UTC) and forecasts (03:00, 09:00, 15:00, 21:00 UTC) and interpolated  
33 on a 1°x1° global longitude-latitude grid. The methodology used here basically consists in releasing  
34 along each vertical profile 1000 particles every 10 hPa and following them backward in time during  
35 20 days. This duration corresponds approximately to the time during which a pollution plume is

1 expected to remain significantly higher than the tropospheric background (Stohl et al., 2003a). The  
2 FLEXPART model computes the particles' residence time, sometimes referred as the potential  
3 emissions sensitivity (PES), that is the potential to catch up emissions from certain regions. Output  
4 are given on a  $1^\circ \times 1^\circ$  global longitude-latitude grid, over 1-km width vertical layers up to 11 km  
5 plus a remaining layer ranging from 11 to 50 km (i.e., 12 vertical layers). The PES between 0-1 km  
6 is presented in Fig. 2 for each tropospheric layer, averaged over the period 1994-2012. As expected,  
7 air masses sampled in the LT spend most of their time in the European BL (mostly in France,  
8 Germany, Benelux, England). In the MT, the influence of Europe persists but the influence of North  
9 America is greatly enhanced. In the UT, the PES is the highest over North America but stronger  
10 winds at these altitudes (e.g. jet streams) also allow a fast transport of air masses from Asia.



11  
12 Figure 2: Average residence time in the first kilometre (normalized by the air density) of air masses  
13 sampled in all three tropospheric layers around Frankfurt. The average is calculated based on all the  
14 FLEXPART simulations over the period 1994-2012. Note the irregular scale.

### 15 **3 Results**

16 The climatological vertical profiles of  $O_3$  and CO around Frankfurt/Munich are described in Sect.  
17 3.1. The annual and monthly variations of both compounds are analysed in Sect. 3.2. The annual  
18 and seasonal trends are investigated in Sect. 3.3. The changes of the  $O_3$  seasonal cycle are explored  
19 in Sect. 3.4.

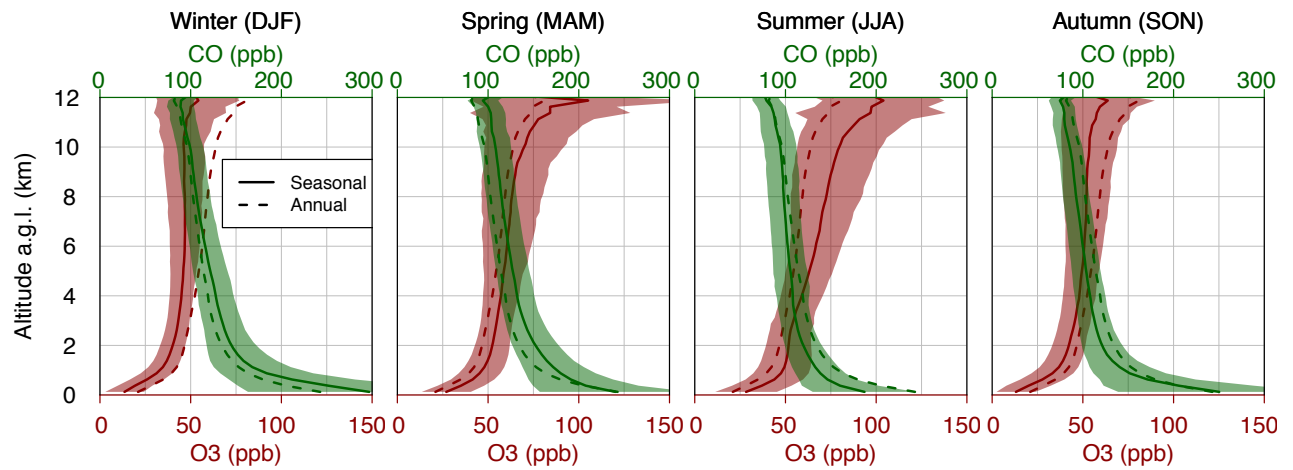


## 1 3.1 Climatological vertical profiles

### 2 3.1.1 Ozone

3 Annual and seasonal mean vertical profiles of O<sub>3</sub> and CO are calculated over the whole period  
4 (1994-2012 for O<sub>3</sub>, 2002-2012 for CO) and shown in Fig. 3. The standard deviation shown in Fig. 3  
5 is inferred from the daily mean vertical profiles, and thus represents the daily variability at the  
6 seasonal scale. Over the entire tropospheric column, the annual mean O<sub>3</sub> mixing ratio is 56 ppb. The  
7 mean O<sub>3</sub> over the tropospheric column shows the minimum mixing ratios in winter (44 ppb) and  
8 autumn (48 ppb), and the maximum ones in summer (67 ppb) and spring (61 ppb). The annual mean  
9 O<sub>3</sub> mixing ratio increases with altitude, from 21 ppb at ground to 81 ppb at 12 km (47 ppb at 2 km).  
10 The highest vertical gradients are found close to the surface (due to dry deposition and enhanced  
11 titration by NO in the BL) during the whole year and close to 12 km during spring and summer (due  
12 to STE). The inflexion of vertical gradients at about 1 km a.g.l. has already been mentioned in  
13 Chevalier et al. (2007). Above 3 km, the mean vertical gradients are +1.1, +1.5, +3.0 and +5.1 ppb  
14 km<sup>-1</sup> in winter, autumn, spring and summer, respectively.

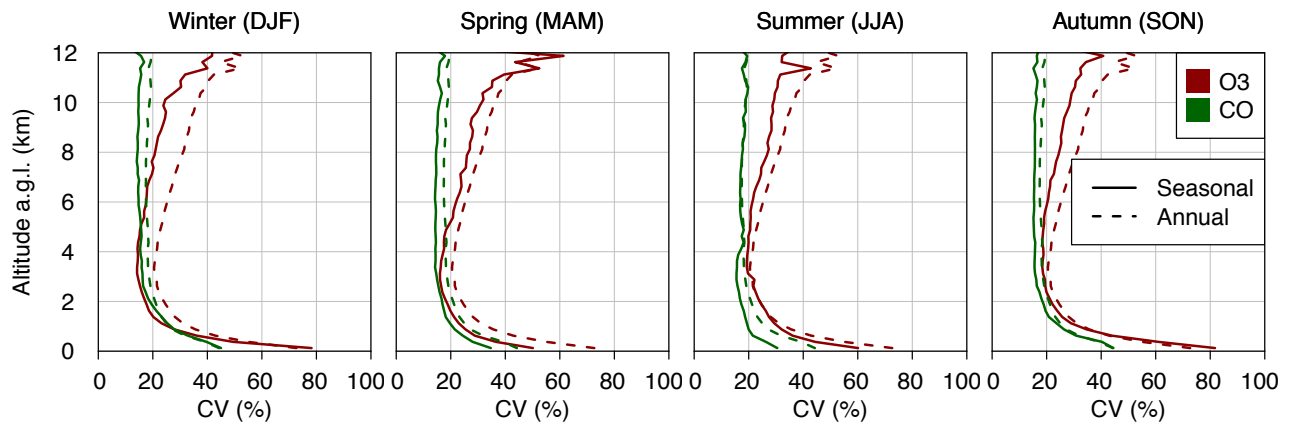
15 During the summer, O<sub>3</sub> episodes are often observed in the European BL (van Loon et al., 2007;  
16 Meleux et al., 2007). High O<sub>3</sub> mixing ratios are also measured in urban environments, despite the  
17 presence of NO<sub>x</sub> emitted locally by the anthropogenic activities (Vautard et al., 2007 reported a 95<sup>th</sup>  
18 percentile of daily O<sub>3</sub> maximum ranging between 70 and 100 ppb in 4 European megacities in  
19 2010). Thus, one might have expected higher mixing ratios in the BL than in the lower free  
20 troposphere (sometimes described as a « C » shaped profile). However, observations do not show  
21 such a profile. One may suspect that this is due to the night-time titration of O<sub>3</sub> in the BL but  
22 limiting data to the afternoon does not highlight a clear « C » shaped profile. Actually, such « C »  
23 shaped profile is only observed when considering the 95<sup>th</sup> percentile rather than the mean O<sub>3</sub> mixing  
24 ratio (Petetin et al., Diurnal cycle of ozone throughout the troposphere over Frankfurt as measured  
25 by MOZAIC-IAGOS commercial aircraft, under review in *Elementa Science of the Anthropocene*).  
26 It means that the potentially high O<sub>3</sub> pollution in the BL during the summer can greatly modify the  
27 vertical profile of O<sub>3</sub> mixing ratios but only episodically. On average, the structure of the mean O<sub>3</sub>  
28 vertical profile in summer remains qualitatively the same (i.e. positive gradient through the whole  
29 troposphere) as during the rest of the year.



1  
 2 Figure 3: Climatological vertical profiles of O<sub>3</sub> and CO mixing ratios above Frankfurt/Munich per  
 3 season (continuous lines). Standard deviation inferred from daily averaged profiles is also indicated  
 4 (filled contour), as well as the annual mean profile (dotted line, the same for all panels).

5 To further characterize the variability of O<sub>3</sub> and CO above Frankfurt/Munich, we now investigate  
 6 the daily variability at both the annual and seasonal scales. The daily variability is here defined as  
 7 the coefficient of variation (CV) of the daily-averaged mixing ratios, that is the standard deviation  
 8 normalized by the corresponding (i.e. annual or seasonal) mean mixing ratio. Vertical profiles of  
 9 the daily variability for O<sub>3</sub> and CO are shown in Fig. 4. Results about CO will be discussed in  
 10 Sect. 3.1.2. The daily variability of O<sub>3</sub> at the annual scale ranges between 20 and 73% depending  
 11 on the altitude, with a mean value of 32%. The maximum daily variability of O<sub>3</sub> is found at  
 12 ground (73%) and at 12 km (53%) where it is likely driven by intense shallow and transient  
 13 exchanges between the stratosphere and the troposphere (Stohl et al., 2003b). Conversely, the  
 14 minimum daily variability is found at about 3.4 km. Such daily variability is lower at the seasonal  
 15 scale, at most altitudes and during most seasons, but the shape of the vertical profiles remains  
 16 similar. The seasonal daily variability minimizes at 4.4 km in autumn and between 3.1-3.4 km  
 17 during the other seasons, thus close to the minimum annual diurnal variability. Similarly, it  
 18 maximizes at the surface and close to the tropopause. Interestingly, the daily variability above 11  
 19 km is noticeably higher in spring than during the other seasons, which again may be due to the day-  
 20 to-day variability of STE that peaks during that season.

1



2

3 Figure 4: Annual (dotted lines, the same for all panels) and seasonal (continuous lines) daily  
4 variability of O<sub>3</sub> and CO mixing ratios above Frankfurt/Munich. The daily variability is here  
5 defined as the coefficient of variation (CV) of the daily-averaged mixing ratios (i.e. the standard  
6 deviation normalized by the mean).

7

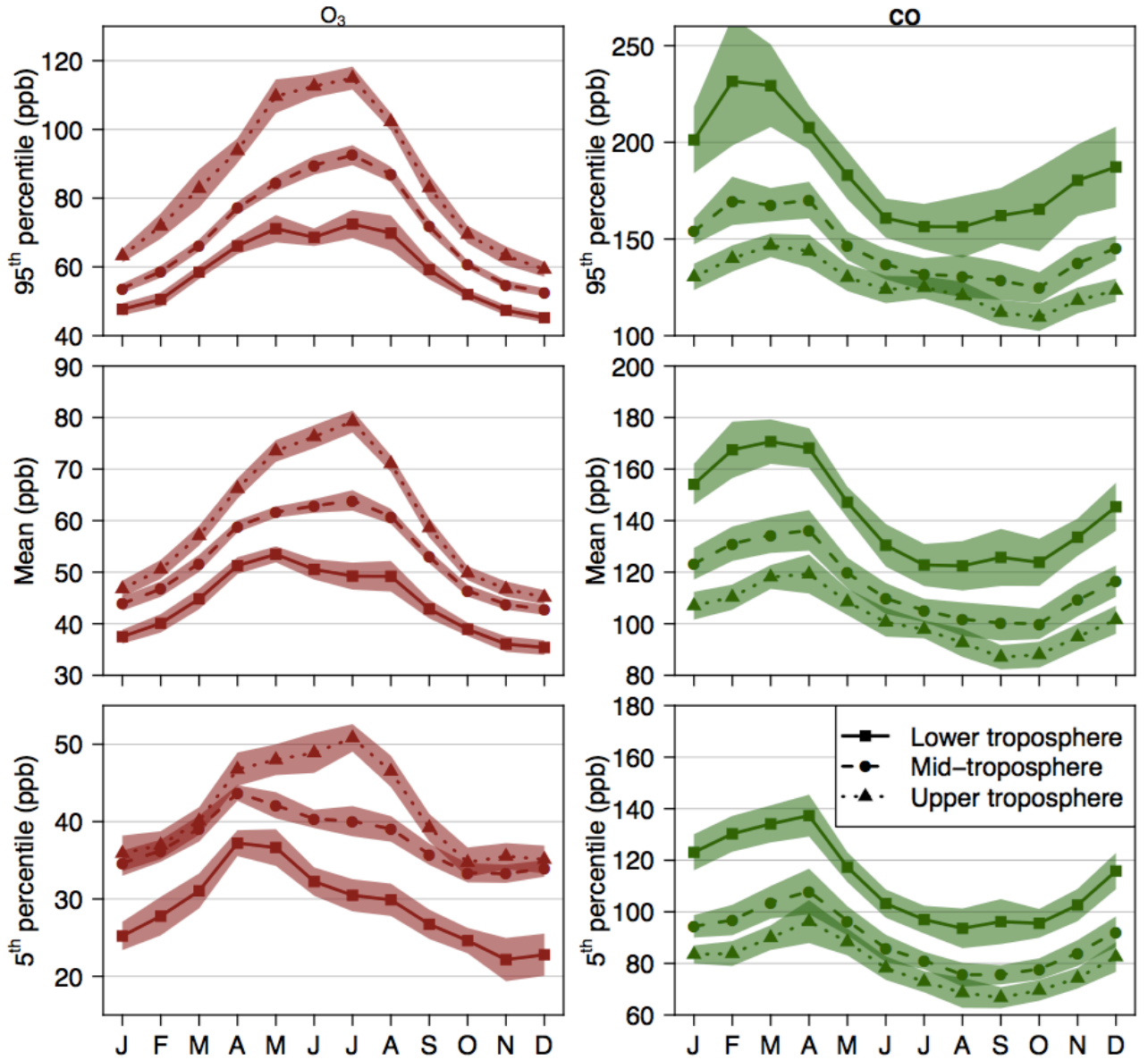
### 8 3.1.2 Carbon monoxide

9 The annual mean vertical profile of CO (Fig. 3) shows mixing ratios ranging from 150 ppb at 1 km  
10 to 80 ppb at 12 km. Over the entire tropospheric column, the mean CO mixing ratio is 117 ppb. At  
11 the ground and close to surface emissions, CO maximizes with 243 ppb on the annual average. This  
12 high mixing ratio is first and foremost due to emissions from the airport area (including aircraft  
13 emissions on runways) and potentially to emissions from the neighbouring agglomeration. The  
14 strongest seasonal variation is observed close to the surface, with mean mixing ratios in the first  
15 kilometre ranging from 156 ppb in summer to 233 ppb in winter. This increase during winter is  
16 likely due to higher emissions and a lower vertical mixing.

17 The Figure 4 shows that the daily variability is lower for CO than for O<sub>3</sub>, in particular at the surface  
18 and close to the tropopause. Over the entire tropospheric column, the annual daily variability of CO  
19 is 20%. It ranges between 44% close to the surface and 17% in the free troposphere where it  
20 remains almost constant with altitude. A very similar picture is drawn for the different seasons. The  
21 highest values at the surface (in the second half of the troposphere) are encountered in  
22 winter/autumn (summer).

### 23 3.2 Annual and monthly variations

24 The average seasonal variations of O<sub>3</sub> and CO in all three tropospheric layers around  
25 Frankfurt/Munich are given in Fig. 5, and their long-term time series are shown in Fig. 6.



1  
 2 Figure 5: Averaged O<sub>3</sub> (left panels) and CO (right panels) seasonal variations above  
 3 Frankfurt/Munich in all three tropospheric layers, for the 95<sup>th</sup> percentile (top panels), the mean  
 4 (middle panels) and the 5<sup>th</sup> percentile (bottom panels). The shaded areas show the  $\pm 2$  standard error  
 5 (i.e. the uncertainty in the average at a 95% confidence level).

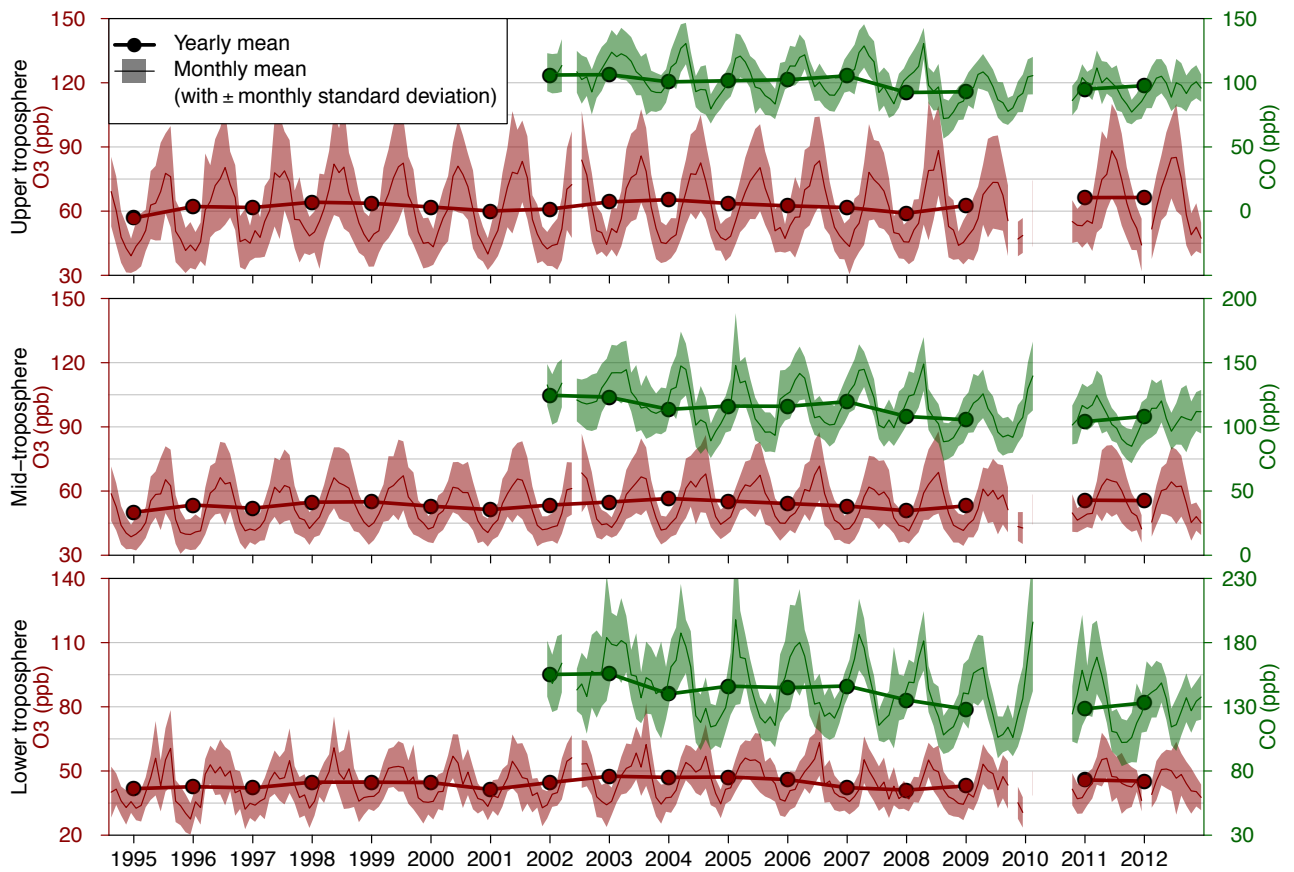
### 6 3.2.1 Ozone

7 As noted in Sect. 3.1.1, the mean tropospheric O<sub>3</sub> increases with altitude, with average mixing ratios  
 8 (over the whole period) of 44, 53 and 63 ppb in the LT, MT and UT, respectively. A clear seasonal  
 9 pattern is emphasized in the entire tropospheric column. In the LT, the seasonal variation shows a  
 10 broad spring/summer maximum and a minimum in winter, in good accordance with the seasonal  
 11 variations observed at surface in Europe (Wilson et al., 2012). In the MT and UT, mixing ratios  
 12 maximize between May and August. The O<sub>3</sub> 5<sup>th</sup> percentile shows higher mixing ratios in April-May  
 13 in the LT and MT while the seasonal variations in the UT remains similar than for the mean O<sub>3</sub>. The

1 95<sup>th</sup> percentile shows a maximum in spring/summer in all tropospheric layers, this maximum being  
2 sharper in the UT than in the LT and MT.

3 The highest monthly mean mixing ratios in the LT (above 60 ppb, the 99<sup>th</sup> percentile) are observed  
4 in August 1995, May 1998, August 2003, July 2006 (Fig. 6). The spring 1998 anomaly is related to  
5 the 1997 El Niño that enhanced the pollution export from Asia (due to a higher convective activity  
6 and a strengthening of the subtropical jet stream) and North America and may have increased the  
7 STE (Koumoutsaris et al., 2008; Zeng and Pyle, 2005). This anomaly is visible in the whole  
8 troposphere, and is the strongest in the UT. The anomalies in August 2003 and July 2006 are related  
9 to the severe heat waves that struck a large part of Europe (Ordóñez et al., 2005; Solberg et al.,  
10 2008; Struzewska and Kaminski, 2008; see also Tressol et al. (2008) for a detailed analysis of the  
11 2003 heat wave with the MOZAIC measurements). They are the strongest in the LT but remain  
12 visible in the MT.

13 The annual mean O<sub>3</sub> mixing ratios are highly correlated between the three tropospheric layers  
14 ( $R=0.87$ ,  $0.75$  and  $0.94$  between the LT/MT, LT/UT and MT/UT, respectively). As the sources and  
15 sinks of O<sub>3</sub> in the troposphere strongly vary with altitude, such high correlations were not expected.  
16 This may be explained by the fact that both the first kilometre and the tropopause layer are not  
17 taken into account in this study, which likely greatly reduces the differences of interannual variation  
18 among the tropospheric layers as defined in this study. In addition, as shown in Sect. 2.2, the  
19 altitude of the UT (defined here based on the PV values) is biased low compared to the UT derived  
20 based on the chemical tropopause. Thus, the UT may be less influenced by the stratosphere and  
21 more by the free troposphere, which may increase the correlation between the MT and UT. Similar  
22 correlations are obtained at the seasonal scale. An interesting exception is the low correlation found  
23 between the LT and UT in summer ( $R=0.26$ ) and spring ( $0.46$ ). This may be due to the fact that the  
24 BL is deeper during these seasons, which keeps away the 1-2 km LT from the influence of the free  
25 troposphere.



1  
 2 Figure 6: Monthly and yearly mean O<sub>3</sub> and CO mixing ratios of combined Frankfurt and Munich  
 3 vertical profiles, in the lower (bottom panel), mid- (middle panel) and upper troposphere (top panel)  
 4 between 1994 and 2012.

### 5 3.2.2 Carbon monoxide

6 On average, CO mixing ratios of 143, 115 and 101 ppb are found in the LT, MT and UT,  
 7 respectively. Mixing ratios in the UT are thus only 29% lower than in the LT close to local  
 8 emissions. In comparison with O<sub>3</sub>, the monthly mean of the daily variability of CO is lower and  
 9 similar in all three tropospheric layers (around 14-16%). Such a result is expected due to the longer  
 10 lifetime of CO in comparison with O<sub>3</sub> in most of the troposphere, which leads to a higher regional  
 11 and hemispheric background (Junge, 1974). As shown in Fig. 5, the seasonal cycle of CO is  
 12 characterized by maximum mixing ratios in late winter/early spring in the whole troposphere.  
 13 Minimum mixing ratios are encountered in summer/early autumn in the LT and are slightly shifted  
 14 to late summer/early autumn higher in altitude. Such a seasonal pattern is consistent with the  
 15 seasonal variation observed in background air masses arriving at the coastal site Mace Head  
 16 (Derwent et al., 1998) or at a larger scale by satellite observations (Edwards et al., 2004; Worden et  
 17 al., 2013). Averaged over the western Europe, the Terra/MOPITT CO tropospheric column  
 18 maximizes at  $\sim 2.5 \cdot 10^{18}$  molecules cm<sup>-2</sup> in March-April and minimize at  $\sim 1.9 \cdot 10^{18}$  molecules cm<sup>-2</sup> in  
 19 late summer, the ratio of the maximum over the minimum being 1.3 (Edwards et al., 2004). A very  
 20 similar seasonal variation of tropospheric columns of CO has been observed by Zbinden et al.

1 (2013) based on the MOZAIC data over the period 2002-2009. This is in good agreement with the  
2 amplitude of the seasonal cycle observed in the MT, the maximum CO mixing ratio being 1.35  
3 higher than the minimum. The winter-time maximum results from the accumulation of the primary  
4 CO emissions at northern mid-latitudes when the photolysis is limited. In summer, CO mixing  
5 ratios minimize due to a more effective photolytic destruction, despite an enhanced secondary  
6 formation from biogenic compounds and additional emissions from biomass burning (in particular  
7 in boreal regions). A rather similar seasonal pattern is observed with the CO 5<sup>th</sup> and 95<sup>th</sup> percentiles  
8 except that the peak is sharper (February-March) in the LT for the 95<sup>th</sup> percentile.

9 As mentioned in Sect. 2.2 and 3.1.2, the data below 1 km were skipped in order to reduce the  
10 impact of the local emissions from both the neighbouring agglomeration and the other aircraft — on  
11 tarmac and/or during the take-off/landing phases (in case the MOZAIC-IAGOS aircraft closely  
12 follows other aircraft). Indeed, many studies have shown that airport activities can impact the air  
13 quality at the local scale (e.g. Hu et al., 2009; Pison and Menut, 2004; Yu et al., 2004). It is worth  
14 mentioning that in a standard landing take-off cycle – comprising the approach, the taxi (plane on  
15 the tarmac), the take-off (acceleration phase on the tarmac) and the climb up to a standard  
16 atmospheric boundary layer of 915 m (Kesgin, 2006) – most of the CO emissions (85-95%) occur  
17 on the tarmac during the taxi phase (Kurniawan and Khardi, 2011). However, even above 1 km in  
18 the LT, one cannot exclude any influence of these emissions, or by the emissions of the  
19 neighbouring agglomeration.

20 To assess more precisely the spatial representativeness of the MOZAIC-IAGOS data in the LT and  
21 MT, a comparison is made with the CO mixing ratios measured at the World Meteorology  
22 Organisation (WMO) Global Atmosphere Watch (GAW) surface stations (see Sect. S.1 in the  
23 Supplement for details). Only the stations located between 45°N and 55°N (i.e.  $\pm 5^\circ$  from the  
24 latitude of Frankfurt) and with at least 80% data capture for the period 2002-2012 (based on the  
25 monthly time series) are retained, which gives a set of 10 stations. The annual mean CO mixing  
26 ratio measured by MOZAIC-IAGOS aircraft in the LT (143 ppb) is in the lower range of the zonal  
27 average  $155 \pm 28$  ppb observed among the GAW surface stations. When considering only the stations  
28 above 1000 m (i.e. 3 stations all located in Europe), the zonal average is reduced to  $145 \pm 19$  ppb,  
29 which is very close to the mean CO observed in the LT. In the MT, the annual mean CO mixing  
30 ratio is 115 ppb, thus lower than the CO mixing ratios at the ground whatever the station, but the  
31 difference with the highest mountain station Jungfrauoch (3580 m elevation) is very small (-7%).  
32 Additionally, the annual MOZAIC-IAGOS CO data in both the LT and MT is strongly correlated  
33 with the CO observed at the ground (R between 0.61 and 0.94 at all stations except one at which  
34  $R=0.41$ ). Therefore, the comparison between the MOZAIC-IAGOS CO dataset at Frankfurt/Munich  
35 and the GAW dataset at the same latitude shows a good consistency, both in terms of mean annual

1 CO mixing ratios and interannual variations. This ensures a satisfactory representativeness of the  
2 MOZAIC-IAGOS observations.

3 Along the period 2002-2012, the highest CO annual mixing ratios are encountered in 2003. This is  
4 in agreement with the satellite measurements that show on this year a high positive anomaly on CO  
5 total columns in Europe and more generally in North Hemisphere, notably due to intense boreal  
6 fires (Worden et al., 2013). High mixing ratios in the LT are also observed during the winter 2010,  
7 concomitantly with a cold snap over Europe that may have induced higher CO emissions (for the  
8 residential heating) (Cattiaux et al., 2010).

### 9 **3.3 Trends**

10 In order to easily compare trends between the different tropospheric layers, O<sub>3</sub> mixing ratios are  
11 normalized following the approach of Parrish et al. (2014) : (i) a quadratic least-squares regression  
12 is applied to mean annual mixing ratios in which the year 2000 is taken as a reference (i.e. the  
13 origin of the time series), (ii) the obtained intercept corresponds to the interpolated mean annual O<sub>3</sub>  
14 mixing ratio in 2000 (hereafter designated as O<sub>3,2000</sub>), and is used for the normalization. Trends are  
15 thus expressed in percentage of year 2000 intercept per year (hereafter referred as %O<sub>3,2000</sub> yr<sup>-1</sup>).  
16 The same approach is used for each season. Considering the relatively short time coverage of  
17 MOZAIC-IAGOS observations (in comparison with measurements at some historical surface sites  
18 traditionally used for long-term trend calculations), we limit the analysis to linear regressions.  
19 Besides mean O<sub>3</sub> mixing ratios, we also investigate trends of the 5<sup>th</sup> and 95<sup>th</sup> percentiles. Hereafter,  
20 all these quantities are referred as M(O<sub>3</sub>), P<sub>5</sub>(O<sub>3</sub>) and P<sub>95</sub>(O<sub>3</sub>) for clarity. The same approach is  
21 followed for CO, with the year 2004 as a reference (and the results expressed in %CO<sub>2004</sub> yr<sup>-1</sup>). This  
22 year is chosen because in all three tropospheric layers, the mean CO mixing ratios in 2004 (140,  
23 114 and 101 ppb in the LT, MT and UT, respectively) are very close to the mean CO mixing ratios  
24 over the period 2002-2012 (141, 114 and 102 ppb). Ozone and CO normalized mean mixing ratios  
25 at the annual and seasonal scale are shown in Fig. S4 in the Supplement (similar plots of the 5<sup>th</sup> and  
26 95<sup>th</sup> percentile are given in Fig. S5-S6 in the Supplement).

27 Trends are investigated using the non-parametric Mann-Kendall analysis combined with Theil-Sen  
28 slope estimate (Sen, 1968) which has several important advantages compared to the least-square  
29 regression, including the absence of distributional assumptions and the lower sensitivity to outliers.  
30 We use the OpenAir package (in the statistical programming language R) developed for  
31 applications in atmospheric sciences (Carslaw and Ropkins, 2012). This package provides an  
32 estimation of the uncertainties based on the bootstrap method, and allows to take into account the  
33 autocorrelation of the data. The autocorrelation of environmental parameters is quite common  
34 (although often ignored in trend analysis), and tends to artificially decrease the uncertainties of  
35 trends, which can lead to the identification of trends that are actually insignificant (Weatherhead et



1 al., 2002). Note that using our approach, the confidence intervals are not necessarily symmetric  
 2 (around the mean slope estimate). The Theil-Sen slope estimates are reported for CO in Table 1. For  
 3 information, the trend uncertainties obtained for O<sub>3</sub> and CO by ignoring the autocorrelation are  
 4 reported in Table S1 in the Supplement.

5 Table 1: Annual and seasonal trends of mean CO mixing ratios, 5<sup>th</sup> and 95<sup>th</sup> percentiles over the  
 6 period 2002-2012. Trends are estimated using the Theil-Sen slope estimate (see text). Uncertainties  
 7 are given at the 95% confidence level (NS: non-significant trend).

		CO relative trend (%CO <sub>2004</sub> yr <sup>-1</sup> )			CO absolute trend (ppb yr <sup>-1</sup> )		
Season	Layer	Mean	5 <sup>th</sup>	95 <sup>th</sup>	Mean	5 <sup>th</sup>	95 <sup>th</sup>
Year	UT	-1.36 [-2.05;-0.74]	-1.22 [-2.27;-0.47]	-1.43 [-2.08;-0.89]	-1.42 [-2.14;-0.78]	-0.91 [-1.69;-0.35]	-2.00 [-2.90;-1.24]
Year	MT	-1.55 [-2.34;-0.72]	-1.57 [-2.52;-0.68]	-1.44 [-2.25;-0.59]	-1.85 [-2.79;-0.85]	-1.33 [-2.15;-0.58]	-2.30 [-3.59;-0.95]
Year	LT	-1.51 [-2.42;-0.44]	-1.59 [-2.58;-0.46]	-1.41 [-2.40;-0.12]	-2.24 [-3.59;-0.65]	-1.69 [-2.75;-0.49]	-2.90 [-4.91;-0.25]
Winter	UT	-1.64 [-2.73;-0.80]	-1.39 [-2.76;-0.39]	-1.59 [-2.59;-1.06]	-1.84 [-3.06;-0.89]	-1.22 [-2.42;-0.34]	-2.20 [-3.60;-1.47]
Winter	MT	-1.50 [-2.53;-0.60]	-1.69 [-2.81;-0.31]	-1.22 [-2.24;-0.28]	-1.96 [-3.29;-0.78]	-1.68 [-2.80;-0.31]	-2.00 [-3.66;-0.45]
Winter	LT	NS	NS	NS	NS	NS	NS
Spring	UT	-1.67 [-2.83;-0.48]	NS	-1.97 [-3.13;-0.86]	-2.02 [-3.43;-0.58]	NS	-2.92 [-4.65;-1.28]
Spring	MT	-2.00 [-2.97;-0.69]	NS	-2.01 [-2.71;-1.07]	-2.76 [-4.09;-0.95]	NS	-3.45 [-4.66;-1.85]
Spring	LT	-1.91 [-2.72;-1.09]	NS	-2.22 [-4.04;-0.87]	-3.26 [-4.64;-1.86]	NS	-4.94 [-9.00;-1.94]
Summer	UT	NS	NS	-1.53 [-2.22;-0.59]	NS	NS	-1.94 [-2.83;-0.75]
Summer	MT	-1.83 [-3.25;-0.56]	NS	-2.29 [-3.77;-1.21]	-2.01 [-3.58;-0.62]	NS	-3.22 [-5.30;-1.70]
Summer	LT	-2.31 [-3.61;-0.97]	-2.08 [-2.83;-0.76]	-2.63 [-4.54;-1.42]	-3.08 [-4.81;-1.29]	-2.16 [-2.94;-0.79]	-4.45 [-7.69;-2.40]
Autumn	UT	NS	NS	NS	NS	NS	NS
Autumn	MT	NS	NS	NS	NS	NS	NS
Autumn	LT	NS	NS	NS	NS	NS	NS

### 1 3.3.1 Ozone

2 All the annual and seasonal trends of the  $M(O_3)$  appear insignificant, except in winter for which a  
3 weakly significant increase is found in all three tropospheric layers ( $+0.83[+0.13;+1.67]$ ,  
4  $+0.62[+0.05;+1.22]$  and  $+0.62[+0.02;+1.22]\%O_{3,2000} \text{ yr}^{-1}$  in the LT, MT and UT, respectively).  
5 Previous trend analysis at the alpine sites (Zugspitze since 1978, Jungfraujoch and Sonnblick since  
6 1990) have highlighted (i) a strong increase of  $O_3$  during all seasons in the 1980s (around  $+0.6-0.9$   
7  $\text{ppb yr}^{-1}$ ), (ii) a persistent but lower increase in the 1990s during all seasons except summer where  
8  $O_3$  has levelled off, (iii) the extension of that levelling off in the 2000s to the other seasons and a  
9 slight decrease in summer (Logan et al., 2012; Parrish et al., 2012). This picture is in general  
10 agreement with our results in the lower part of the troposphere. More specifically, in winter, Parrish  
11 et al. (2012) found an average trend of  $+0.61\pm 0.25 \%O_{3,2000} \text{ yr}^{-1}$  at regional background sites in  
12 Europe over the 2-3 last decades, which is consistent with the trends found here over the period  
13 1994-2012. At low altitudes, this increase of  $O_3$  in winter is mainly attributed to a reduced  $O_3$   
14 titration by  $NO$  due to decreasing  $NO_x$  emissions (e.g. Ordóñez et al., 2005). The persistent positive  
15 trends found higher in altitude suggest that wintertime  $O_3$  has increased at a large scale (if not  
16 hemispheric) since air masses sampled by MOZAIC-IAGOS aircraft in both the MT and UT can be  
17 influenced by emissions from North America and Asia (as shown in Fig. 2).

18 Concerning the  $P_5(O_3)$ , a significant increase is found at the annual scale in all three tropospheric  
19 layers ( $+1.03[+0.36;+1.62]$ ,  $+0.42[+0.09;+0.68]$  and  $+0.63[+0.09;+0.99]\%O_{3,2000} \text{ yr}^{-1}$  in the LT, MT  
20 and UT, respectively). Conversely, trends of the  $P_{95}(O_3)$  are all insignificant. Note that ignoring the  
21 autocorrelation of the data leads to some additional significant positive trends, including the  $M(O_3)$   
22 at the annual scale, the  $P_5(O_3)$  in winter and autumn, and the  $P_{95}(O_3)$  in winter, although not in all  
23 tropospheric layers (see Table S1 in the Supplement). It is beyond the scope of this study to  
24 investigate why the autocorrelation has a stronger effect on these specific seasons or layers, but this  
25 illustrates the strong influence of the serial dependence on the trend analysis and the necessity to  
26 take it into account.

### 27 3.3.2 Carbon monoxide

28 As previously mentioned in the beginning of Sect. 3.3,  $CO$  trends are here investigated relatively to  
29 the 2004 reference year. Over the period 2002-2012, the  $M(CO)$  at the annual scale significantly  
30 decreases in the whole troposphere, with trends of  $-1.51[-2.42;-0.44]$ ,  $-1.55[-2.34;-0.72]$  and  $-1.36[-$   
31  $2.05;-0.74]\%CO_{2004} \text{ yr}^{-1}$  in the LT, MT and UT, respectively. Similar negative trends are also  
32 obtained for the  $P_5(CO)$  and  $P_{95}(CO)$  in all the tropospheric layers. At the seasonal scale, the  $M(CO)$   
33 and  $P_{95}(CO)$  show negative trends in winter, spring and summer, although not always in all the  
34 tropospheric layers, while the  $P_5(CO)$  is significantly decreasing in winter (in the MT and UT) and  
35 summer (in the LT). Conversely, all trends in autumn are insignificant. Note that the results without

1 taking into consideration the autocorrelation of the data show significant negative trends of the  
2  $P_5(\text{CO})$  in most layers and during all the seasons, except autumn (see Table S1 in the Supplement).  
3 These results are in general agreement with previous studies in Europe (e.g., Karlsdóttir et al., 2000;  
4 Novelli et al., 2003; Dils et al., 2009; Worden et al., 2013). Based on satellite observations, Worden  
5 et al. (2013) highlighted over Europe a decrease of the CO total columns, around  $-1.44 \pm 0.22\% \text{ yr}^{-1}$   
6 with MOPITT over 2001-2011 and  $-1.00 \pm 0.33\% \text{ yr}^{-1}$  with AIRS over 2003-2011, thus in the range  
7 of our results over Frankfurt. Over the period 1995-2007, Gilge et al. (2010) found trends of -  
8  $3.36 \pm 1.08$  and  $-1.51 \pm 0.64 \text{ ppb yr}^{-1}$  (reduced to  $-2.65 \pm 0.04 \text{ ppb yr}^{-1}$  by filtering the background  
9 values (Zellweger et al., 2009)) at two alpine sites from the WMO GAW network, in reasonable  
10 agreement with our absolute Theil-Sen slope estimates at Frankfurt/Munich in the LT and MT (-  
11  $2.24[-3.59;-0.65]$  and  $-1.85[-2.79;-0.85] \text{ ppb yr}^{-1}$ ).

### 12 **3.4 Changes of the O<sub>3</sub> seasonal cycle**

13 In Sect. 3.3.1, we highlighted that only a few O<sub>3</sub> trends are statistically significant. However, the  
14 differences of trends between the seasons remain insignificant. It is worth noting that an  
15 insignificant trend does not imply the absence of trend since a trend can be hidden by a strong  
16 variability. In this section, we investigate if these trends come along with a change of the O<sub>3</sub>  
17 seasonal cycle above Frankfurt/Munich (Sect. 3.4.1). Results are discussed in Sect. 3.4.2.

#### 18 **3.4.1 Evolution of the seasonal cycle at Frankfurt/Munich**

19 The seasonal variation of O<sub>3</sub> can be well approximated by a sine function fully characterized by  
20 three parameters: an offset value defined here as the average O<sub>3</sub> mixing ratio over the considered  
21 period, an amplitude, and a phase that determines at which period in the year the maximum of O<sub>3</sub> is  
22 reached. Following the approach of Parrish et al. (2013), one can fit a sine function over different  
23 periods of time and compare the results of the fit in order to highlight potential changes in the  
24 seasonal pattern of O<sub>3</sub>. While Parrish et al. (2013) applied the sine fit to the monthly mean time  
25 series, we here consider the daily mean O<sub>3</sub> mixing ratio but the results from both approaches will be  
26 discussed. The equation of the fit is :

$$27 \tilde{y}(t) = y_0 + a \sin\left(\frac{2\pi t}{365} + \phi\right) \quad (1)$$

28 with  $t$  the time (in days, values ranging between 0.5 and 364.5),  $y_0$  the offset mixing ratio (in ppb),  $a$   
29 the amplitude (in ppb) and  $\phi$  the phase. The date of the year of the seasonal maximum of O<sub>3</sub> is then  
30 estimated as :  $(\pi/2 - \phi) * 365/2\pi$  (Parrish et al., 2013). We apply the sine fit on the two 9-year  
31 time periods 1995-2003 and 2004-2012. As there is no overlap between these periods, the two  
32 datasets and the results of the sine fit are independent. The changes of amplitude and phase obtained  
33 with the sine fits are reported in Table 2.

1 Between 1995-2003 and 2004-2012, the amplitude of the O<sub>3</sub> seasonal cycle has significantly  
 2 decreased in the whole troposphere, with a rate of decrease of  $-2.5\pm 0.9$ ,  $-1.1\pm 0.5$  and  $-2.1\pm 1.0$  ppb  
 3 decade<sup>-1</sup> in the LT, MT and UT, respectively. Reason for the decreasing amplitude is the  
 4 significantly increased yearly O<sub>3</sub> minimum occurring in winter and to the same time constant O<sub>3</sub>  
 5 maximum occurring in spring/summer (see Sect. 3.3.1). The differences of amplitude change  
 6 between the different layers all remain statistically insignificant.

7 Table 2. Characteristics of the O<sub>3</sub> seasonal cycle over the periods 1995-2003 and 2004-2012 in all  
 8 tropospheric layers. Amplitude and phase are obtained by fitting a sine function on the daily mean  
 9 O<sub>3</sub> mixing ratios (see text).

Layer	Amplitude			Phase		
	Amplitude 1995-2003 (ppb)	Amplitude 2004-2012 (ppb)	Amplitude trend (ppb decade <sup>-1</sup> )	Date of seasonal maximum 1995- 2003	Date of seasonal maximum 2004- 2012	Shift (day decade <sup>-1</sup> )
UT	18.0±0.7	16.1±0.6	-2.1±1.0	23 June ± 2 days	20 June ± 2 days	-3.3±3.3
MT	11.5±0.3	10.5±0.3	-1.1±0.5	23 June ± 1 days	16 June ± 2 days	-7.8±2.5
LT	9.9±0.6	7.6±0.5	-2.5±0.9	18 June ± 3 days	2 June ± 4 days	-17.8±6.0

10 Over the period 1995-2003, the sine fit gives a seasonal maximum of O<sub>3</sub> the 18 June in the LT and  
 11 the 23 June in the MT and UT. The date of seasonal maximum in the LT is in reasonable agreement  
 12 with those obtained by Parrish et al. (2013) at two alpine sites (Jungfrauoch, Switzerland and  
 13 Zugspitze, Germany) and at a lower elevation site (Hohenpeissenberg, Germany, ~50 km from  
 14 Munich). Over the period 2004-2012, the seasonal maximum O<sub>3</sub> occurs the 2 June in the LT, the 16  
 15 June in the MT and the 20 June in the UT. Thus, the phase of the seasonal variations of O<sub>3</sub> shifted  
 16 forward during the period 1995-2012. The seasonal shift between 1995-2003 and 2004-2012 is  
 17 highly significant in the LT ( $-17.8\pm 6.0$  day decade<sup>-1</sup>) and MT ( $-7.8\pm 2.5$  day decade<sup>-1</sup>), and nearly  
 18 insignificant in the UT ( $-3.3\pm 3.3$  day decade<sup>-1</sup>). The differences of seasonal shift between the  
 19 tropospheric layers are all significant, and the seasonal shift thus decreases with altitude. Note that  
 20 applying the sine fit to the monthly O<sub>3</sub> mixing ratios give similar shift estimates but much larger  
 21 uncertainties, leading to insignificant differences among the tropospheric layers ( $-13.3\pm 11.6$  and  
 22  $-6.7\pm 6.5$  day decade<sup>-1</sup> in the LT and MT, respectively). Note that reducing the width of the time  
 23 windows (to less than 9 years) does not give significantly different results.

24 At the three continental sites, Parrish et al. (2013) reported statistically significant rates of shift (at  
 25 the 95% confidence level) ranging between -5 and -7 days decade<sup>-1</sup> since 1970s while at the coastal

1 site Mace Head, the rate was lower and insignificant ( $-3\pm 3.7$  days decade<sup>-1</sup>). In comparison, the  
2 seasonal shift we obtained in the LT is significantly higher, but discrepancies are likely due to the  
3 fact that the studied periods are different. As a faster change of phase is found between 2005 and  
4 2008 (the 3 last years studied) (see Fig. 2 in Parrish et al. (2013)), restricting their analysis to our  
5 shorter period would likely lead to a higher seasonal shift (i.e., closer to our values).

### 6 **3.4.2 Discussion**

7 This previous analysis confirms that the ozone seasonal pattern in Central/Western Europe is  
8 changing, at least since the mid-1990s, moving toward a lower amplitude and an earlier O<sub>3</sub>  
9 maximum. It is worth noting that the MOZAIC-IAGOS observations above Frankfurt/Munich  
10 represent the worldwide densest dataset of O<sub>3</sub> vertical profiles, which gives robustness to our results.  
11 Thanks to vertical profile observations, it brings an interesting contribution by showing that this  
12 seasonal change of the phase above Frankfurt/Munich decreases with altitude. This may highlight  
13 that the O<sub>3</sub> seasonal pattern behave differently over the northern hemisphere continents (Europe,  
14 North America, Asia). Indeed, the FLEXPART-derived PES clearly shows that the air masses  
15 sampled by MOZAIC-IAGOS aircraft in the different tropospheric layers originate from different  
16 regions (see Fig. 2). The LT is predominantly influenced by the European emissions, the MT by  
17 both the European and Northern American emissions, the UT by both the Northern American and  
18 Asian emissions.

19 Parrish et al. (2013) exhaustively discussed several reasons that may explain this changing phase at  
20 surface in Europe, including changes in downward transport of stratospheric O<sub>3</sub>, long-range  
21 transport, O<sub>3</sub> precursor's emissions and their spatial distribution, photochemical production and the  
22 potential influence of climate change. Our study does not provide an unambiguous explanation to  
23 either the seasonal trends discrepancies or the subsequent seasonal shifts (which would ideally  
24 require the use of global models able to correctly reproduce both O<sub>3</sub> seasonal patterns and trends  
25 throughout the troposphere). In terms of stratospheric contributions, the STE is known to peak in  
26 spring (Auvray and Bey, 2005; James et al., 2003; Tang et al., 2011) due to both enhanced  
27 downward transport (Appenzeller et al., 1996) and maximum mixing ratios in the lowermost  
28 stratosphere (e.g., Thouret et al., 2006). If the seasonal shift was induced by higher STT fluxes, one  
29 would expect stronger positive trends in spring close to the tropopause compared to the LT and a  
30 larger (and more significant) seasonal shift in the UT, which contradicts our observations. Thus, the  
31 STE is not likely the main reason explaining the shift of the O<sub>3</sub> seasonal pattern. The trend analysis  
32 (Sect. 3.3) has not highlighted any significant O<sub>3</sub> trend either in spring or summer, the large  
33 uncertainties being at least partly due to the strong interannual variability of O<sub>3</sub> mixing ratios.

## 1 **4 Summary and conclusions**

2 An extensive database of O<sub>3</sub> and CO vertical profiles above worldwide airports is available from the  
3 MOZAIC-IAGOS program since 1994 and 2002, respectively. In this study, we investigate the  
4 climatology, variations and trends of O<sub>3</sub> and CO mixing ratios above the German airports Frankfurt  
5 and Munich whose combination represents the worldwide densest and longest MOZAIC-IAGOS  
6 dataset. We focus on the troposphere, each vertical profile being subdivided in three tropospheric  
7 layers: the lower, mid- and upper troposphere (LT, MT and UT, respectively). The UT is defined  
8 relative to the dynamical tropopause, based on the potential vorticity extracted from ECMWF  
9 meteorological data. Main results are given below (all trends are given with uncertainties at a 95%  
10 confidence level):

- 11 1. Climatological vertical profiles: The mean O<sub>3</sub> vertical profile is characterized by a strong  
12 increase with altitude in the first kilometre above the surface whatever the season and close  
13 to the tropopause in spring/summer, while the vertical gradient remains moderate (low) in  
14 the free troposphere in spring/summer (winter/autumn). These variations of the O<sub>3</sub> vertical  
15 gradient are likely due to the effect of deposition and titration by NO close to the surface,  
16 and STE close to the tropopause. We also highlighted a minimum of daily O<sub>3</sub> variability at  
17 around 3-4 km. The mean CO vertical profile shows maximum mixing ratios at the surface,  
18 a strong decrease in the first kilometre (in particular in winter/autumn) and a moderate one  
19 in the rest of the troposphere. A maximum of variability is also found at the surface, while  
20 that variability remains constant (around 18%) through the rest of the troposphere, whatever  
21 the season.
- 22 2. Seasonal variations: The mean O<sub>3</sub> seasonal variations show a minimum in November-  
23 December in all tropospheric layers, a broad spring/summer maximum in the LT and MT  
24 and a sharper summer maximum in the UT. The O<sub>3</sub> 5<sup>th</sup> percentile is also minimum in  
25 November-December in all the troposphere, but reaches its maximum in April-May in the  
26 LT and MT, and April-August in the UT. The seasonal profile of the O<sub>3</sub> 95<sup>th</sup> percentile is  
27 less contrasted in the troposphere, with a maximum in April-August in the LT, July-August  
28 in the MT and May-July in the UT. The mean CO seasonal variations peak in March/April  
29 in the whole troposphere, and reach a broad minimum in July-October in the LT, refined to  
30 September/October in the MT and UT. A similar pattern is observed for the CO 5<sup>th</sup> and 95<sup>th</sup>  
31 percentiles.
- 32 3. Annual and seasonal O<sub>3</sub> trends: Over the period 1994-2012, most O<sub>3</sub> trends are insignificant.  
33 The few exceptions are the significant increases of the mean O<sub>3</sub> in winter, and of the O<sub>3</sub> 5<sup>th</sup>  
34 percentile at the annual scale. No significant trends are found for the O<sub>3</sub> 95<sup>th</sup> percentile.  
35 Considering the uncertainties at a 95% confidence level, the significant trend values range

1 between 0.02 and 1.67%O<sub>3,2000</sub> yr<sup>-1</sup> (relative change with the year 2000 as a reference). Over  
2 the period 2002-2012, the mean CO mixing ratios are decreasing at the annual scale and at  
3 the seasonal scale in winter, spring and summer in all the tropospheric layers (except in the  
4 LT in winter), with trends ranging between -2.31[-3.61;-0.97] and -1.36[-2.05;-  
5 0.74]%CO<sub>2004</sub> yr<sup>-1</sup> (relative change with the year 2004 as a reference). A similar picture is  
6 observed for both the 5<sup>th</sup> and the 95<sup>th</sup> percentiles, except that most trends in spring and  
7 summer are insignificant for the 5<sup>th</sup> percentile. All trends remain insignificant in autumn.

8 This study also investigates the changes in the O<sub>3</sub> seasonal cycle (by fitting sinusoids over the 9-  
9 years periods 1995-2003 and 2004-2012) with a focus on the phase. Results highlight a statistically  
10 significant change of the phase in the LT, ozone maxima occurring earlier by -17.8±6.0 days  
11 decade<sup>-1</sup> on average (at a 95% confidence level), in general agreement with previous results from  
12 the literature (Parrish et al., 2013). A major contribution of this study concerns the dependence on  
13 altitude of this seasonal shift, as it is found to decrease with altitude, with -7.8±2.5 days decade<sup>-1</sup> in  
14 the mid-troposphere and -3.3±3.3 days decade<sup>-1</sup> in the upper troposphere (i.e. nearly insignificant).  
15 The larger contribution from other regions (e.g. Asia) higher in altitude may explain the lower  
16 seasonal shift observed in the UT, although further studies are obviously required to quantitatively  
17 assess this issue.

## 18 **Acknowledgements**

19 The authors acknowledge the strong support of the European Commission, Airbus, and the Airlines  
20 (Lufthansa, Air-France, Austrian, Air Namibia, Cathay Pacific, Iberia and China Airlines so far)  
21 who carry the MOZAIC or IAGOS equipment and perform the maintenance since 1994. In its last  
22 10 years of operation, MOZAIC has been funded by INSU-CNRS (France), Météo-France,  
23 Université Paul Sabatier (Toulouse, France) and Research Center Jülich (FZJ, Jülich, Germany).  
24 IAGOS has been additionally funded by the EU projects IAGOS-DS and IAGOS-ERI. The  
25 MOZAIC-IAGOS database is supported by AERIS (CNES and INSU-CNRS). Data are also  
26 available via AERIS web site [www.aeris-data.fr](http://www.aeris-data.fr). We are very thankful to the referees for their  
27 numerous recommendations that greatly helped us to improve this paper.

## 28 **References**

- 29 Appenzeller, C., Holton, J. R. and Rosenlof, K. H.: Seasonal variation of mass transport across the  
30 tropopause, *J. Geophys. Res. Atmos.*, 101(D10), 15071–15078, doi:10.1029/96JD00821, 1996.
- 31 Ashmore, M. R.: Assessing the future global impacts of ozone on vegetation, *Plant, Cell Environ.*,  
32 28(8), 949–964, doi:10.1111/j.1365-3040.2005.01341.x, 2005.
- 33 Auvray, M. and Bey, I.: Long-range transport to Europe: Seasonal variations and implications for

1 the European ozone budget, *J. Geophys. Res.*, 110(D11), D11303, doi:10.1029/2004JD005503,  
2 2005.

3 Bethan, S., Vaughan, G. and Reid, S. J.: A comparison of ozone and thermal tropopause heights and  
4 the impact of tropopause definition on quantifying the ozone content of the troposphere, *Q. J. R.*  
5 *Meteorol. Soc.*, 122(532), 929–944, doi:10.1002/qj.49712253207, 1996.

6 Carslaw, D. C. and Ropkins, K.: openair — An R package for air quality data analysis, *Environ.*  
7 *Model. Softw.*, 27-28, 52–61, doi:10.1016/j.envsoft.2011.09.008, 2012.

8 Cattiaux, J., Vautard, R., Cassou, C., Yiou, P., Masson-Delmotte, V. and Codron, F.: Winter 2010  
9 in Europe: A cold extreme in a warming climate, *Geophys. Res. Lett.*, 37(20), n/a–n/a,  
10 doi:10.1029/2010GL044613, 2010.

11 Chevalier, A., Gheusi, F., Delmas, R., Ordóñez, C., Sarrat, C., Zbinden, R., Thouret, V., Athier, G.  
12 and Cousin, J.-M.: Influence of altitude on ozone levels and variability in the lower troposphere: a  
13 ground-based study for western Europe over the period 2001–2004, *Atmos. Chem. Phys.*, 7(16),  
14 4311–4326, doi:10.5194/acp-7-4311-2007, 2007.

15 Cooper, O. R., Parrish, D. D., Ziemke, J., Balashov, N. V., Cupeiro, M., Galbally, I. E., Gilge, S.,  
16 Horowitz, L., Jensen, N. R., Lamarque, J.-F., Naik, V., Oltmans, S. J., Schwab, J., Shindell, D. T.,  
17 Thompson, A. M., Thouret, V., Wang, Y. and Zbinden, R. M.: Global distribution and trends of  
18 tropospheric ozone: An observation-based review, *Elem. Sci. Anthr.*, 2, 000029,  
19 doi:10.12952/journal.elementa.000029, 2014.

20 Cui, J., Pandey Deolal, S., Sprenger, M., Henne, S., Staehelin, J., Steinbacher, M. and Nédélec, P.:  
21 Free tropospheric ozone changes over Europe as observed at Jungfraujoch (1990–2008): An  
22 analysis based on backward trajectories, *J. Geophys. Res.*, 116(D10), D10304,  
23 doi:10.1029/2010JD015154, 2011.

24 Derwent, R. G., Simmonds, P. G., Seuring, S. and Dimmer, C.: Observation and interpretation of  
25 the seasonal cycles in the surface concentrations of ozone and carbon monoxide at mace head,  
26 Ireland from 1990 to 1994, *Atmos. Environ.*, 32(2), 145–157, doi:10.1016/S1352-2310(97)00338-5,  
27 1998.

28 Derwent, R. G., Manning, A. J., Simmonds, P. G., Spain, T. G. and O’Doherty, S.: Analysis and  
29 interpretation of 25 years of ozone observations at the Mace Head Atmospheric Research Station on  
30 the Atlantic Ocean coast of Ireland from 1987 to 2012, *Atmos. Environ.*, 80, 361–368,  
31 doi:10.1016/j.atmosenv.2013.08.003, 2013.

32 Van Dingenen, R., Dentener, F. J., Raes, F., Krol, M. C., Emberson, L. and Cofala, J.: The global  
33 impact of ozone on agricultural crop yields under current and future air quality legislation, *Atmos.*  
34 *Environ.*, 43(3), 604–618, doi:10.1016/j.atmosenv.2008.10.033, 2009.

35 Edwards, D. P., Emmons, L. K., Hauglustaine, D. A., Chu, D. A., Gille, J. C., Kaufman, Y. J., Ieron,  
36 G. P., Yurganov, L. N., Giglio, L., Deeter, M. N., Yudin, V., Ziskin, D. C., Warner, J., Lamarque,



1 J.-F., Francis, G. L., Ho, S. P., Mao, D., Chen, J., Grechko, E. I. and Drummond, J. R.:  
2 Observations of carbon monoxide and aerosols from the Terra satellite: Northern Hemisphere  
3 variability, *J. Geophys. Res.*, 109(D24), D24202, doi:10.1029/2004JD004727, 2004.  
4 Gaudel, A., Ancellet, G. and Godin-Beekmann, S.: Analysis of 20 years of tropospheric ozone  
5 vertical profiles by lidar and ECC at Observatoire de Haute Provence (OHP) at 44°N, 6.7°E, *Atmos.*  
6 *Environ.*, 113, 78–89, doi:10.1016/j.atmosenv.2015.04.028, 2015.  
7 Gilge, S., Plass-Duelmer, C., Fricke, W., Kaiser, A., Ries, L., Buchmann, B. and Steinbacher, M.:  
8 Ozone, carbon monoxide and nitrogen oxides time series at four alpine GAW mountain stations in  
9 central Europe, *Atmos. Chem. Phys.*, 10(24), 12295–12316, doi:10.5194/acp-10-12295-2010, 2010.  
10 Hu, S., Fruin, S., Kozawa, K., Mara, S., Winer, A. M. and Paulson, S. E.: Aircraft Emission Impacts  
11 in a Neighborhood Adjacent to a General Aviation Airport in Southern California, *Environ. Sci.*  
12 *Technol.*, 43(21), 8039–8045, doi:10.1021/es900975f, 2009.  
13 IPCC: Climate change 2013 : The physical science basis., 2013.  
14 James, P., Stohl, A., Forster, C., Eckhardt, S., Seibert, P. and Frank, A.: A 15-year climatology of  
15 stratosphere-troposphere exchange with a Lagrangian particle dispersion model: 1. Methodology  
16 and validation, *J. Geophys. Res.*, 108(D12), 8519, doi:10.1029/2002JD002637, 2003.  
17 Jerrett, M., Burnett, R. T., Pope, C. A., Ito, K., Thurston, G., Krewski, D., Shi, Y., Calle, E. and  
18 Thun, M.: Long-term ozone exposure and mortality., *N. Engl. J. Med.*, 360(11), 1085–95,  
19 doi:10.1056/NEJMoa0803894, 2009.  
20 Junge, C. E.: Residence time and variability of tropospheric trace gases, *Tellus*, 26(4), 477–488,  
21 doi:10.1111/j.2153-3490.1974.tb01625.x, 1974.  
22 Karlsdóttir, S., Isaksen, I. S. A., Myhre, G. and Berntsen, T. K.: Trend analysis of O<sub>3</sub> and CO in  
23 the period 1980–1996: A three-dimensional model study, *J. Geophys. Res.*, 105(D23), 28907,  
24 doi:10.1029/2000JD900374, 2000.  
25 Kesgin, U.: Aircraft emissions at Turkish airports, *Energy*, 31(2-3), 372–384,  
26 doi:10.1016/j.energy.2005.01.012, 2006.  
27 Koumoutsaris, S., Bey, I., Generoso, S. and Thouret, V.: Influence of El Niño–Southern Oscillation  
28 on the interannual variability of tropospheric ozone in the northern midlatitudes, *J. Geophys. Res.*,  
29 113(D19), D19301, doi:10.1029/2007JD009753, 2008.  
30 Kunz, A., Konopka, P., Müller, R. and Pan, L. L.: Dynamical tropopause based on isentropic  
31 potential vorticity gradients, *J. Geophys. Res.*, 116(D1), D01110, doi:10.1029/2010JD014343, 2011.  
32 Kurniawan, J. S. and Khardi, S.: Comparison of methodologies estimating emissions of aircraft  
33 pollutants, environmental impact assessment around airports, *Environ. Impact Assess. Rev.*, 31(3),  
34 240–252, doi:10.1016/j.eiar.2010.09.001, 2011.  
35 Logan, J. A., Megretskaia, I. A., Miller, A. J., Tiao, G. C., Choi, D., Zhang, L., Stolarski, R. S.,  
36 Labow, G. J., Hollandsworth, S. M., Bodeker, G. E., Claude, H., De Muer, D., Kerr, J. B., Tarasick,

1 D. W., Oltmans, S. J., Johnson, B., Schmidlin, F., Staehelin, J., Viatte, P. and Uchino, O.: Trends in  
2 the vertical distribution of ozone: A comparison of two analyses of ozonesonde data, *J. Geophys.*  
3 *Res.*, 104(D21), 26373, doi:10.1029/1999JD900300, 1999.

4 Logan, J. A., Staehelin, J., Megretskaia, I. A., Cammas, J.-P., Thouret, V., Claude, H., De Backer,  
5 H., Steinbacher, M., Scheel, H.-E., Stübi, R., Fröhlich, M. and Derwent, R.: Changes in ozone over  
6 Europe: Analysis of ozone measurements from sondes, regular aircraft (MOZAIC) and alpine  
7 surface sites, *J. Geophys. Res.*, 117(D9), D09301, doi:10.1029/2011JD016952, 2012.

8 van Loon, M., Vautard, R., Schaap, M., Bergström, R., Bessagnet, B., Brandt, J., Builtjes, P. J. H.,  
9 Christensen, J. H., Cuvelier, C., Graff, a., Jonson, J. E., Krol, M., Langner, J., Roberts, P., Rouil, L.,  
10 Stern, R., Tarrasón, L., Thunis, P., Vignati, E., White, L. and Wind, P.: Evaluation of long-term  
11 ozone simulations from seven regional air quality models and their ensemble, *Atmos. Environ.*,  
12 41(10), 2083–2097, doi:10.1016/j.atmosenv.2006.10.073, 2007.

13 Marengo, A., Thouret, V., Nédélec, P., Smit, H., Helten, M., Kley, D., Karcher, F., Simon, P., Law,  
14 K., Pyle, J., Poschmann, G., Von Wrede, R., Hume, C. and Cook, T.: Measurement of ozone and  
15 water vapor by Airbus in-service aircraft: The MOZAIC airborne program, an overview, *J. Geophys.*  
16 *Res. Atmos.*, 103(D19), 25631–25642, doi:10.1029/98JD00977, 1998.

17 Meleux, F., Solmon, F. and Giorgi, F.: Increase in summer European ozone amounts due to climate  
18 change, *Atmos. Environ.*, 41(35), 7577–7587, doi:10.1016/j.atmosenv.2007.05.048, 2007.

19 Moise, T. and Rudich, Y.: Reactive uptake of ozone by proxies for organic aerosols: Surface versus  
20 bulk processes, *J. Geophys. Res.*, 105(D11), 14667, doi:10.1029/2000JD900071, 2000.

21 Moise, T. and Rudich, Y.: Reactive Uptake of Ozone by Aerosol-Associated Unsaturated Fatty  
22 Acids: Kinetics, Mechanism, and Products, *J. Phys. Chem. A*, 106(27), 6469–6476,  
23 doi:10.1021/jp025597e, 2002.

24 Nédélec, P., Cammas, J.-P., Thouret, V., Athier, G., Cousin, J.-M., Legrand, C., Abonnel, C.,  
25 Lecoeur, F., Cayez, G. and Marizy, C.: An improved infrared carbon monoxide analyser for routine  
26 measurements aboard commercial Airbus aircraft: technical validation and first scientific results of  
27 the MOZAIC III programme, *Atmos. Chem. Phys.*, 3(5), 1551–1564, doi:10.5194/acp-3-1551-2003,  
28 2003.

29 Nédélec, P., Blot, R., Boulanger, D., Athier, G., Cousin, J.-M., Gautron, B., Petzold, A., Volz-  
30 Thomas, A. and Thouret, V.: Instrumentation on commercial aircraft for monitoring the  
31 atmospheric composition on a global scale: the IAGOS system, technical overview of ozone and  
32 carbon monoxide measurements, *Tellus B*, 67, 1–16, doi:10.3402/tellusb.v67.27791, 2015.

33 Novelli, P. C., Masarie, K. A., Lang, P. M., Hall, B. D., Myers, R. C. and Elkins, J. W.: Reanalysis  
34 of tropospheric CO trends: Effects of the 1997–1998 wildfires, *J. Geophys. Res.*, 108(D15), 4464,  
35 doi:10.1029/2002JD003031, 2003.

36 Oltmans, S. J., Lefohn, A. S., Scheel, H. E., Harris, J. M., Levy, H., Galbally, I. E., Brunke, E.-G.,

1 Meyer, C. P., Lathrop, J. A., Johnson, B. J., Shadwick, D. S., Cuevas, E., Schmidlin, F. J., Tarasick,  
2 D. W., Claude, H., Kerr, J. B., Uchino, O. and Mohnen, V.: Trends of ozone in the troposphere,  
3 *Geophys. Res. Lett.*, 25(2), 139–142, doi:10.1029/97GL03505, 1998.

4 Oltmans, S. J., Lefohn, A. S., Harris, J. M., Galbally, I., Scheel, H. E., Bodeker, G., Brunke, E.,  
5 Claude, H., Tarasick, D., Johnson, B. J., Simmonds, P., Shadwick, D., Anlauf, K., Hayden, K.,  
6 Schmidlin, F., Fujimoto, T., Akagi, K., Meyer, C., Nichol, S., Davies, J., Redondas, A. and Cuevas,  
7 E.: Long-term changes in tropospheric ozone, *Atmos. Environ.*, 40(17), 3156–3173,  
8 doi:10.1016/j.atmosenv.2006.01.029, 2006.

9 Oltmans, S. J., Lefohn, A. S., Shadwick, D., Harris, J. M., Scheel, H. E., Galbally, I., Tarasick, D.  
10 W., Johnson, B. J., Brunke, E.-G., Claude, H., Zeng, G., Nichol, S., Schmidlin, F., Davies, J.,  
11 Cuevas, E., Redondas, A., Naoe, H., Nakano, T. and Kawasato, T.: Recent tropospheric ozone  
12 changes - A pattern dominated by slow or no growth, *Atmos. Environ.*, 67, 331–351,  
13 doi:10.1016/j.atmosenv.2012.10.057, 2013.

14 Ordóñez, C., Mathis, H., Furger, M., Henne, S., Hüglin, C., Staehelin, J. and Prévôt, A. S. H.:  
15 Changes of daily surface ozone maxima in Switzerland in all seasons from 1992 to 2002 and  
16 discussion of summer 2003, *Atmos. Chem. Phys.*, 5(5), 1187–1203, doi:10.5194/acp-5-1187-2005,  
17 2005.

18 Paoletti, E.: Impact of ozone on Mediterranean forests: a review., *Environ. Pollut.*, 144(2), 463–74,  
19 doi:10.1016/j.envpol.2005.12.051, 2006.

20 Parrish, D. D., Law, K. S., Staehelin, J., Derwent, R., Cooper, O. R., Tanimoto, H., Volz-Thomas,  
21 A., Gilge, S., Scheel, H.-E., Steinbacher, M. and Chan, E.: Long-term changes in lower  
22 tropospheric baseline ozone concentrations at northern mid-latitudes, *Atmos. Chem. Phys.*, 12(23),  
23 11485–11504, doi:10.5194/acp-12-11485-2012, 2012.

24 Parrish, D. D., Law, K. S., Staehelin, J., Derwent, R., Cooper, O. R., Tanimoto, H., Volz-Thomas,  
25 A., Gilge, S., Scheel, H.-E., Steinbacher, M. and Chan, E.: Lower tropospheric ozone at northern  
26 midlatitudes: Changing seasonal cycle, *Geophys. Res. Lett.*, 40(8), 1631–1636,  
27 doi:10.1002/grl.50303, 2013.

28 Parrish, D. D., Lamarque, J.-F., Naik, V., Horowitz, L., Shindell, D. T., Staehelin, J., Derwent, R.,  
29 Cooper, O. R., Tanimoto, H., Volz-Thomas, A., Gilge, S., Scheel, H.-E., Steinbacher, M. and  
30 Fröhlich, M.: Long-term changes in lower tropospheric baseline ozone concentrations: Comparing  
31 chemistry-climate models and observations at northern midlatitudes, *J. Geophys. Res. Atmos.*,  
32 119(9), 5719–5736, doi:10.1002/2013JD021435, 2014.

33 Petzold, A., Thouret, V., Gerbig, C., Zahn, A., Brenninkmeijer, C. A. M., Gallagher, M., Hermann,  
34 M., Pontaud, M., Ziereis, H., Boulanger, D., Marshall, J., Nédélec, P., Smit, H. G. J., Friess, U.,  
35 Flaud, J.-M., Wahner, A., Cammas, J.-P. and Volz-Thomas, A.: Global-scale atmosphere  
36 monitoring by in-service aircraft – current achievements and future prospects of the European

1 Research Infrastructure IAGOS, *Tellus B*, 67, 1–24, doi:10.3402/tellusb.v67.28452, 2015.

2 Pison, I. and Menut, L.: Quantification of the impact of aircraft traffic emissions on tropospheric  
3 ozone over Paris area, *Atmos. Environ.*, 38(7), 971–983, doi:10.1016/j.atmosenv.2003.10.056, 2004.

4 Sen, P. K.: Estimates of the Regression Coefficient Based on Kendall’s Tau, *J. Am. Stat. Assoc.*,  
5 63(324), 1379–1389, doi:10.1080/01621459.1968.10480934, 1968.

6 Simmonds, P. G., Derwent, R. G., Manning, A. L. and Spain, G.: Significant growth in surface  
7 ozone at Mace Head, Ireland, 1987–2003, *Atmos. Environ.*, 38(28), 4769–4778,  
8 doi:10.1016/j.atmosenv.2004.04.036, 2004.

9 Solberg, S., Hov, Ø., Søvde, A., Isaksen, I. S. A., Coddeville, P., De Backer, H., Forster, C.,  
10 Orsolini, Y. and Uhse, K.: European surface ozone in the extreme summer 2003, *J. Geophys. Res.*,  
11 113(D7), D07307, doi:10.1029/2007JD009098, 2008.

12 Staufer, J., Staehelin, J., Stübi, R., Peter, T., Tummon, F. and Thouret, V.: Trajectory matching of  
13 ozonesondes and MOZAIC measurements in the UTLS &ndash; Part 1: Method description  
14 and application at Payerne, Switzerland, *Atmos. Meas. Tech.*, 6(12), 3393–3406, doi:10.5194/amt-  
15 6-3393-2013, 2013.

16 Staufer, J., Staehelin, J., Stübi, R., Peter, T., Tummon, F. and Thouret, V.: Trajectory matching of  
17 ozonesondes and MOZAIC measurements in the UTLS – Part 2: Application to the global  
18 ozonesonde network, *Atmos. Meas. Tech.*, 7(1), 241–266, doi:10.5194/amt-7-241-2014, 2014.

19 Stevenson, D. S., Dentener, F. J., Schultz, M. G., Ellingsen, K., van Noije, T. P. C., Wild, O., Zeng,  
20 G., Amann, M., Atherton, C. S., Bell, N., Bergmann, D. J., Bey, I., Butler, T., Cofala, J., Collins, W.  
21 J., Derwent, R. G., Doherty, R. M., Drevet, J., Eskes, H. J., Fiore, A. M., Gauss, M., Hauglustaine,  
22 D. A., Horowitz, L. W., Isaksen, I. S. A., Krol, M. C., Lamarque, J.-F., Lawrence, M. G.,  
23 Montanaro, V., Müller, J.-F., Pitari, G., Prather, M. J., Pyle, J. A., Rast, S., Rodriguez, J. M.,  
24 Sanderson, M. G., Savage, N. H., Shindell, D. T., Strahan, S. E., Sudo, K. and Szopa, S.:  
25 Multimodel ensemble simulations of present-day and near-future tropospheric ozone, *J. Geophys.*  
26 *Res.*, 111(D8), D08301, doi:10.1029/2005JD006338, 2006.

27 Stohl, A., Forster, C., Eckhardt, S., Spichtinger, N., Huntrieser, H., Heland, J., Schlager, H.,  
28 Wilhelm, S., Arnold, F. and Cooper, O.: A backward modeling study of intercontinental pollution  
29 transport using aircraft measurements, *J. Geophys. Res.*, 108(D12), 4370,  
30 doi:10.1029/2002JD002862, 2003a.

31 Stohl, A., Wernli, H., James, P., Bourqui, M., Forster, C., Liniger, M. A., Seibert, P. and Sprenger,  
32 M.: A New Perspective of Stratosphere–Troposphere Exchange, *Bull. Am. Meteorol. Soc.*, 84(11),  
33 1565–1573, doi:10.1175/BAMS-84-11-1565, 2003b.

34 Stohl, A., Forster, C., Frank, A., Seibert, P. and Wotawa, G.: Technical note: The Lagrangian  
35 particle dispersion model FLEXPART version 6.2, *Atmos. Chem. Phys.*, 5(9), 2461–2474,  
36 doi:10.5194/acp-5-2461-2005, 2005.

1 Struzewska, J. and Kaminski, J. W.: Formation and transport of photooxidants over Europe during  
2 the July 2006 heat wave – observations and GEM-AQ model simulations, *Atmos. Chem. Phys.*,  
3 8(3), 721–736, doi:10.5194/acp-8-721-2008, 2008.

4 Tang, Q., Prather, M. J. and Hsu, J.: Stratosphere-troposphere exchange ozone flux related to deep  
5 convection, *Geophys. Res. Lett.*, 38(3), n/a–n/a, doi:10.1029/2010GL046039, 2011.

6 Tanimoto, H., Zbinden, R. M., Thouret, V. and Nédélec, P.: Consistency of tropospheric ozone  
7 observations made by different platforms and techniques in the global databases, *Tellus B*, 67,  
8 doi:10.3402/tellusb.v67.27073, 2015.

9 Thouret, V., Marengo, A., Logan, J. A., Nédélec, P. and Grouhel, C.: Comparisons of ozone  
10 measurements from the MOZAIC airborne program and the ozone sounding network at eight  
11 locations, *J. Geophys. Res.*, 103(D19), 25695–25720, doi:10.1029/98JD02243, 1998.

12 Thouret, V., Cammas, J.-P., Sauvage, B., Athier, G., Zbinden, R., Nédélec, P., Simon, P. and  
13 Karcher, F.: Tropopause referenced ozone climatology and inter-annual variability (1994–2003)  
14 from the MOZAIC programme, *Atmos. Chem. Phys.*, 6(4), 1033–1051, doi:10.5194/acp-6-1033-  
15 2006, 2006.

16 Tiao, G. C., Reinsel, G. C., Pedrick, J. H., Allenby, G. M., Mateer, C. L., Miller, A. J. and DeLuisi,  
17 J. J.: A statistical trend analysis of ozonesonde data, *J. Geophys. Res.*, 91(D12), 13121,  
18 doi:10.1029/JD091iD12p13121, 1986.

19 Tressol, M., Ordonez, C., Zbinden, R., Brioude, J., Thouret, V., Mari, C., Nedelec, P., Cammas, J.-  
20 P., Smit, H., Patz, H.-W. and Volz-Thomas, A.: Air pollution during the 2003 European heat wave  
21 as seen by MOZAIC airliners, *Atmos. Chem. Phys.*, 8(8), 2133–2150, doi:10.5194/acp-8-2133-  
22 2008, 2008.

23 Vautard, R., Builtjes, P. H. J., Thunis, P., Cuvelier, C., Bedogni, M., Bessagnet, B., Honoré, C.,  
24 Moussiopoulos, N., Pirovano, G. and Schaap, M.: Evaluation and intercomparison of Ozone and  
25 PM10 simulations by several chemistry transport models over four European cities within the  
26 CityDelta project, *Atmos. Environ.*, 41(1), 173–188, doi:10.1016/j.atmosenv.2006.07.039, 2007.

27 Weatherhead, E. C., Stevermer, A. J. and Schwartz, B. E.: Detecting environmental changes and  
28 trends, *Phys. Chem. Earth, Parts A/B/C*, 27(6-8), 399–403, doi:10.1016/S1474-7065(02)00019-0,  
29 2002.

30 Wilson, R. C., Fleming, Z. L., Monks, P. S., Clain, G., Henne, S., Konovalov, I. B., Szopa, S. and  
31 Menut, L.: Have primary emission reduction measures reduced ozone across Europe? An analysis  
32 of European rural background ozone trends 1996–2005, *Atmos. Chem. Phys.*, 12(1), 437–454,  
33 doi:10.5194/acp-12-437-2012, 2012.

34 Worden, H. M., Deeter, M. N., Frankenberg, C., George, M., Nichitiu, F., Worden, J., Aben, I.,  
35 Bowman, K. W., Clerboux, C., Coheur, P. F., de Laat, A. T. J., Detweiler, R., Drummond, J. R.,  
36 Edwards, D. P., Gille, J. C., Hurtmans, D., Luo, M., Martínez-Alonso, S., Massie, S., Pfister, G. and

1 Warner, J. X.: Decadal record of satellite carbon monoxide observations, *Atmos. Chem. Phys.*,  
2 13(2), 837–850, doi:10.5194/acp-13-837-2013, 2013.

3 Wu, S., Mickley, L. J., Jacob, D. J., Logan, J. A., Yantosca, R. M. and Rind, D.: Why are there  
4 large differences between models in global budgets of tropospheric ozone?, *J. Geophys. Res.*,  
5 112(D5), D05302, doi:10.1029/2006JD007801, 2007.

6 Yu, K. N., Cheung, Y. P., Cheung, T. and Henry, R. C.: Identifying the impact of large urban  
7 airports on local air quality by nonparametric regression, *Atmos. Environ.*, 38(27), 4501–4507,  
8 doi:10.1016/j.atmosenv.2004.05.034, 2004.

9 Zbinden, R. M., Cammas, J.-P., Thouret, V., Nédélec, P., Karcher, F. and Simon, P.: Mid-latitude  
10 tropospheric ozone columns from the MOZAIC program: climatology and interannual variability,  
11 *Atmos. Chem. Phys.*, 6(4), 1053–1073, doi:10.5194/acp-6-1053-2006, 2006.

12 Zbinden, R. M., Thouret, V., Ricaud, P., Carminati, F., Cammas, J.-P. and Nédélec, P.: Climatology  
13 of pure tropospheric profiles and column contents of ozone and carbon monoxide using MOZAIC  
14 in the mid-northern latitudes (24° N to 50° N) from 1994 to 2009, *Atmos. Chem. Phys.*, 13(24),  
15 12363–12388, doi:10.5194/acp-13-12363-2013, 2013.

16 Zellweger, C., Hüglin, C., Klausen, J., Steinbacher, M., Vollmer, M. and Buchmann, B.: Inter-  
17 comparison of four different carbon monoxide measurement techniques and evaluation of the long-  
18 term carbon monoxide time series of Jungfraujoch, *Atmos. Chem. Phys.*, 9(11), 3491–3503,  
19 doi:10.5194/acp-9-3491-2009, 2009.

20 Zeng, G. and Pyle, J. A.: Influence of El Niño Southern Oscillation on stratosphere/troposphere  
21 exchange and the global tropospheric ozone budget, *Geophys. Res. Lett.*, 32(1), L01814,  
22 doi:10.1029/2004GL021353, 2005.

23